

# Multipole transitions to determine lifetimes and polarizabilities in Mg-like ions from Si<sup>2+</sup> to Fm<sup>88+</sup>

U. I. Safranova and A. S. Safranova

*Physics Department, University of Nevada, Reno, Nevada 89557, USA*

P. Beiersdorfer

*Physics Division, Lawrence Livermore National Laboratory, Livermore, California 94550, USA*

(Received 14 June 2014; published 21 July 2014)

The relativistic many-body perturbation theory (RMBPT), including the Breit interaction, is used to evaluate the multipole ( $E1$ ,  $M1$ ,  $E2$ ,  $M2$ , and  $E3$ ) matrix elements to determine the  $3s3p\ ^3P_2$  lifetime and multipole polarizabilities in Mg-like ions. The electric multipole matrix elements are determined in length and velocity forms. The calculations start from a  $1s^22s^22p^6$  Dirac-Fock potential. First-order RMBPT is used to obtain intermediate coupling coefficients, and second-order RMBPT is used to calculate transition matrix elements. Contributions from negative-energy states are included in the second-order multipole matrix elements to ensure gauge independence of transition amplitudes. The details of our calculations of the multipole polarizabilities are illustrated for Mg-like Si<sup>2+</sup>, Fe<sup>14+</sup>, Kr<sup>24+</sup>, Mo<sup>30+</sup>, Xe<sup>42+</sup>, and W<sup>62+</sup> ions. Our RMBPT results are compared with available theoretical results and experimental measurements. Trends of the line strengths, transition rates, and contributions in the ground-state multipole polarizabilities as functions of  $Z$  are illustrated graphically in Mg-like ions with  $Z = 14\text{--}100$ .

DOI: [10.1103/PhysRevA.90.012519](https://doi.org/10.1103/PhysRevA.90.012519)

PACS number(s): 31.15.am, 31.15.ag, 31.15.ap

## I. INTRODUCTION

Early work concerning lifetime measurements of Mg-like ions have been presented in a large number of publications [1–27]. Most of those measurements were focused on the  $3s^2$ – $3s3p$  resonance and intercombination transitions: Engström *et al.*, in their discussion of beam-foil Cl VI [26], refer to previous work on these transitions in S V and Ar VII by Reistad *et al.* [17,19] and in Fe XV and Ni XVII by Hutton *et al.* [22,23]. Baudinet-Robinet *et al.* [13] made lifetime measurements of most of the low-lying allowed transitions in Cl VI, while Träbert *et al.* [25] measured the resonance transition lifetime in Br XXIV. Träbert *et al.* [27] made an extensive set of lifetime measurements, including those for the  $3p3d\ ^3F$  states, in Mg-like calcium Ca<sup>8+</sup>.

Very importantly, optical decay rates of the  $3s3p\ ^3P_2$  level in Mg-like ions of  $^{59}\text{Co}^{15+}$ ,  $^{58}\text{Ni}^{16+}$ , and  $^{63,65}\text{Cu}^{17+}$  were recently measured at a heavy-ion storage ring by Träbert *et al.* [28]. It was found that the measurements were sensitive to magnetic dipole ( $M1$ ), magnetic quadrupole ( $M2$ ), and hyperfine-induced decay rates. The measurement precision was just about high enough to detect the difference in the isotope effect on the level lifetime in  $^{63,65}\text{Cu}^{17+}$  ions [28]. The effect of the hyperfine interaction on the lifetime of the  $3s3p\ ^3P_2$  level of Mg-like ions was discussed by Kang *et al.* [29]. Their calculation was performed using the GRASP2K package based on the multiconfiguration Dirac-Hartree-Fock method. Here, the contribution to the lifetime of the  $^3P_2$  level from the  $3s3p\ ^3P_2 \rightarrow 3s^2\ ^1S_0$  hyperfine-induced electric dipole ( $E1$ ),  $3s3p\ ^3P_2 \rightarrow 3s3p\ ^3P_1$   $M1$ ,  $3s3p\ ^3P_2 \rightarrow 3s^2\ ^1S_0$   $M2$ , and  $3s3p\ ^3P_2 \rightarrow 3s3p\ ^3P_{0,1}$  electric quadrupole ( $E2$ ) transition was evaluated for  $^{27}\text{Al}^{1+}$ ,  $^{29}\text{Si}^{2+}$ ,  $^{43}\text{Ca}^{8+}$ ,  $^{57}\text{Fe}^{14+}$ ,  $^{65}\text{Cu}^{17+}$ ,  $^{107}\text{Ag}^{35+}$ , and  $^{173}\text{Yb}^{58+}$  in detail. It was found in [29] that the hyperfine interaction has an obvious effect at the beginning of the Mg-like isoelectronic sequence. The same GRASP2K package was used by Andersson *et al.* to investigate the hyperfine quenching of the two metastable  $3s3p\ ^3P_2$  and

$3s3p\ ^3P_0$  levels in Mg-like ions ranging from  $Z = 12$  to  $Z = 31$  [30]. Energy levels and radiative rates for transitions in Mg-like iron, cobalt, and nickel were evaluated by Aggarwal *et al.* [31], who obtained results for  $E2$ ,  $M1$ , and  $M2$  transitions using the GRASP code.

Recently, the Flexible Atomic Code (FAC) was used by Landi [32] to evaluate oscillator strengths and radiative decay rates for the  $3l3l'$ ,  $3l4l'$ , and  $3l5l'$  states in the Mg-like Fe<sup>14+</sup> ion. Energy levels and radiative rates for  $E1$  transitions among the lowest  $3l3l'$  and  $3l4l'$  levels of Fe XV, Co XVI, and Ni XVII were calculated by Aggarwal *et al.* [31] using the CIV3 code employing extensive configuration-interaction (CI) wave functions. The important relativistic effects were included through the Breit-Pauli approximation. In order to attain calculated energy splittings close to the experimental values, small adjustments were made to the diagonal elements of the Hamiltonian matrices [31]. Excitation energies, transition probabilities, and lifetimes were calculated by Safranova *et al.* for the  $3l_13l_2$ – $3l_33l_4$  electric dipole transitions in Mg-like ions with nuclear charges  $Z$  ranging from 13 to 100 [33]. Relativistic many-body perturbation theory (RMBPT), including the Breit interaction, was used to evaluate retarded  $E1$  matrix elements in length and velocity forms. The calculations start from a  $1s^22s^22p^6$  Dirac-Fock (DF) potential. First-order perturbation theory was used to obtain intermediate coupling coefficients, and the second-order MBPT is used to determine the matrix elements. The contributions from negative-energy states are included in the second-order  $E1$  matrix elements to achieve agreement between length-form and velocity-form amplitudes [33].

Determination of polarizabilities and lifetimes for the Mg isoelectronic sequences was reported by Reshetnikov *et al.* [34]. They suggested that measurements of the lifetime of the lowest resonance transition could be used to specify the polarizabilities and, alternatively, that measurements of the polarizabilities could be used to deduce the lifetimes. Moreover, they

showed that isoelectronic regularities in line strengths can be used to obtain a comprehensive database from a small number of precision lifetime determinations. These methods were applied homologously to produce values for polarizabilities and lifetimes for the Mg, Zn, Cd, and Hg isoelectronic sequences [34]. Static and dynamic polarizabilities of Mg-like ions were investigated by Hamonou and Hibbert [35], who determine the static and frequency-dependent dipole polarizabilities for the ground state of neutral Mg and four ions in the magnesium sequence: Al<sup>+</sup>, Si<sup>2+</sup>, P<sup>3+</sup>, and S<sup>4+</sup>. The wave functions were written in terms of CI expansions. Radial functions of orbitals up to  $n = 9$  were used in the calculations: some optimized on the polarizability, some on the energies of low-lying states [35]. The polarizability of the Si<sup>2+</sup> ion was calculated by Mitroy [36]. In that work, the dipole polarizability of the Si<sup>2+</sup> ground state was determined by a large-scale CI calculation employing the sum-over-states approach. The CI calculation was used to describe the valence electron dynamics with respect to the Hamiltonian, which treats core-valence correlations with a semiempirical approach. Various higher-order polarizabilities were also computed [36]. The dipole polarizability of Si<sup>2+</sup> was measured by Komara *et al.* [37]. Fine-structure intervals connecting  $n = 19$  Rydberg levels of Si<sup>+</sup> with  $L$  between 9 and 16 were measured precisely using the resonant excitation Stark ionization spectroscopy technique. The fine-structure pattern conformed closely to that predicted by an effective potential model and indicated a value of  $11.666(4)a_0^3$  for the adiabatic dipole polarizability of the Mg-like Si<sup>2+</sup> ion [37].

In the present paper, RMBPT is used to determine matrix elements, line strengths, and transition rates for electric multipole ( $E1$ ,  $E2$ , and  $E3$ ) and magnetic multipole ( $M1$ ,  $M2$ , and  $M3$ ) transitions between the  $3l/3l'$  and the  $3l/4l'$  excited states with  $3l = 3s, 3p, 3d$ ,  $3l' = 3s, 3p, 3d$ , and  $4l' = 4s, 4p, 4d, 4f$  in Mg-like ions with a nuclear charge ranging from  $Z = 14$  to  $Z = 100$ . Calculations are carried out to second order in perturbation theory. Lifetimes of the  $3s3p\ ^3P_2$  level and the  $E1$ ,  $E2$ , and  $E3$  multipole polarizabilities are given for  $Z = 14$ –100. Taking into account that calculations have been performed over a very broad range of  $Z$ , most of the data are presented in graphs as  $Z$  dependencies. However, a detailed discussion of the various contributions to the multipole polarizabilities is given for Mg-like silicon, iron, krypton, molybdenum, xenon, and tungsten ( $Z = 14, 26, 36, 42, 54$ , and 74). The relativistic atomic data for these particular ions are important for the study of a variety of laboratory plasmas such as for tokamaks [38,39] and x-ray lasers [40,41].

Unless stated otherwise, we use atomic units (a.u.) for all matrix elements and polarizabilities throughout this paper. The atomic unit for polarizability can be converted to SI units via  $\alpha/h [\text{Hz}/(\text{V/m})^2] = 2.488\ 32 \times 10^{-8}\alpha$  (a.u.), where the conversion coefficient is  $4\pi\epsilon_0a_0^3/h$ , where  $a_0$  is the Bohr radius and  $\epsilon_0$  is the electric constant.

## II. MULTIPOLE MATRIX ELEMENTS BETWEEN TWO EXCITED STATES

The first-order reduced  $N$ -pole matrix element  $T_K^{(1)}$  for transitions between two states,  $vw(J)$  and  $v'w'(J')$ , is

[42,43]

$$\begin{aligned} T_N^{(1)}[v_1w_1(J) - v_2w_2(J')] \\ = \sqrt{[J][J']} \sum_{vw} \sum_{v'w'} S^J(v_1w_1, vw) S^{J'}(v_2w_2, v'w') \\ \times (-1)^{K+j_w+j_{v'}} \left\{ \begin{matrix} J & J' & N \\ j_{v'} & j_w & j_v \end{matrix} \right\} T_N(v'w) \delta_{vw'}, \quad (1) \end{aligned}$$

where  $[J] = 2J + 1$ . The quantity  $S^J(v_1w_1, vw)$  is a symmetry coefficient defined by

$$S^J(v_1w_1, vw) = \eta_{v_1w_1} [\delta_{v_1v}\delta_{w_1w} + (-1)^{j_v+j_w+J+1}\delta_{v_1w}\delta_{w_1v}], \quad (2)$$

where  $\eta_{vw}$  is a normalization factor given by

$$\eta_{vw} = \begin{cases} 1 & \text{for } w \neq v, \\ 1/\sqrt{2} & \text{for } w = v. \end{cases}$$

The electric  $N$ -pole matrix element  $T_N(vw)$ , which includes retardation (see Eqs. (38) and (39) in Ref. [42]),  $T_N(vw) = \frac{(2N+1)!!}{k^N} \langle v \parallel t_N^{(1)} \parallel w \rangle$ , is given in velocity and length forms as

$$\begin{aligned} T_N(vw) = \langle \kappa_v \parallel C_N \parallel \kappa_w \rangle \frac{(2N-1)!!}{k^N} \int_0^\infty dr \left\{ N j_{N-1}(kr) \right. \\ + N j_{N+1}(kr) [G_v(r)F_w(r) - F_v(r)G_w(r)] \\ - \frac{\kappa_v - \kappa_w}{N+1} [(N+1)j_{N-1}(kr) - N j_{N+1}(kr)] \\ \left. \times [G_v(r)F_w(r) + F_v(r)G_w(r)] \right\} \quad (3) \end{aligned}$$

and

$$\begin{aligned} T_N(vw) = \langle \kappa_v \parallel C_N \parallel \kappa_w \rangle \frac{(2N+1)!!}{k^N} \int_0^\infty dr \\ \times \left( j_N(kr) [G_v(r)G_w(r) + F_v(r)F_w(r)] \right. \\ + j_{N+1}(kr) \left\{ \frac{\kappa_v - \kappa_w}{N+1} [G_v(r)F_w(r) + F_v(r)G_w(r)] \right. \\ \left. \left. + [G_v(r)F_w(r) - F_v(r)G_w(r)] \right\} \right), \quad (4) \end{aligned}$$

respectively. The magnetic  $N$ -pole matrix element  $T_N(vw)$ , which includes retardation, is given by

$$\begin{aligned} T_N(vw) = \langle -\kappa_v \parallel C_N \parallel \kappa_w \rangle \frac{2(2N+1)!!}{\alpha k^N} \int_0^\infty dr \frac{\kappa_v + \kappa_w}{N+1} j_N(kr) \\ \times [G_v(r)F_w(r) + F_v(r)G_w(r)]. \quad (5) \end{aligned}$$

Here  $\kappa_v$  is the angular momentum quantum number [ $\kappa_v = \mp(j_v + \frac{1}{2})$  for  $j_v = (l_v \pm \frac{1}{2})$ ] and  $k = \alpha\omega$ , where  $\omega$  is the photon energy:  $\omega = \varepsilon_w - \varepsilon_v$  for  $T_N(vw)$ . The quantity  $C_{1q}(\hat{r})$  is a normalized spherical harmonic. The functions  $G_v(r)$  and  $F_v(r)$  are the large- and small-component radial Dirac wave functions, respectively. The single-particle matrix elements  $Z_{vw}(k)$  reduce to the velocity- and length-form matrix elements of the dipole operator in the limit  $k \rightarrow 0$ .

The second-order reduced matrix element  $T_N^{(2)}$  for the transition between the two states  $vw(J) - v'w'(J')$  consists of four contributions: the DF term [ $T_N^{(\text{DF})}$ ], random-phase approximation (RPA) term [ $T_N^{(\text{RPA})}$ ], correlation contribution [ $T_N^{(\text{corr})}$ ], and derivative term [ $T_N^{(\text{deriv})}$ ]:

$$T_N^{(\text{HF})}[v_1 w_1(J) - v_2 w_2(J')] = \sqrt{[J][J']} \sum_{vw} \sum_{v'w'} \mathcal{S}^J(v_1 w_1, vw) \mathcal{S}^{J'}(v_2 w_2, v'w') \\ \times (-1)^{N+j_w+j_{v'}} \left\{ \begin{array}{ccc} J & J' & N \\ j_{v'} & j_w & j_v \end{array} \right\} \sum_i \left[ \frac{Z_N(v'i)\Delta_{iw}}{\varepsilon_i - \varepsilon_w} + \frac{Z_N(iw)\Delta_{v'i}}{\varepsilon_i - \varepsilon_{v'}} \right] \delta_{vw'}, \quad (6)$$

$$T_N^{(\text{RPA})}[v_1 w_1(J) - v_2 w_2(J')] = \frac{1}{2N+1} \sqrt{[J][J']} \sum_{vw} \sum_{v'w'} \mathcal{S}^J(v_1 w_1, vw) \mathcal{S}^{J'}(v_2 w_2, v'w') (-1)^{j_{w'}+j_v} \left\{ \begin{array}{ccc} J & J' & N \\ j_{v'} & j_w & j_v \end{array} \right\} \\ \times \sum_n \sum_b \left[ \frac{Z_N(bn)Z_N(wbv'n)}{\varepsilon_n + \varepsilon_{v'} - \varepsilon_w - \varepsilon_b} + \frac{Z_N(nb)Z_N(wnv'b)}{\varepsilon_n + \varepsilon_w - \varepsilon_{v'} - \varepsilon_b} \right] \delta_{vw'}, \quad (7)$$

$$T_N^{(\text{corr})}[v_1 w_1(J) - v_2 w_2(J')] = \sqrt{[J][J']} \sum_{vw} \sum_{v'w'} \mathcal{S}^J(v_1 w_1, vw) \mathcal{S}^{J'}(v_2 w_2, v'w') \\ \times \sum_k (-1)^{N+k} \sum_i \left[ \frac{Z_N(iv)X_k(v'w'wi)}{\varepsilon_i + \varepsilon_w - \varepsilon_{v'} - \varepsilon_{w'}} \left\{ \begin{array}{ccc} J & J' & N \\ j_i & j_v & j_w \end{array} \right\} \left\{ \begin{array}{ccc} j_i & j_w & J' \\ j_{v'} & j_{w'} & k \end{array} \right\} (-1)^{j_{w'}+j_{v'}} \right. \\ \left. + \frac{Z_N(v'i)X_k(iw'vw)}{\varepsilon_i + \varepsilon_{w'} - \varepsilon_v - \varepsilon_w} \left\{ \begin{array}{ccc} J' & J & K \\ j_{v'} & j_w & j_{w'} \end{array} \right\} \left\{ \begin{array}{ccc} j_i & j_{w'} & J \\ j_w & j_v & k \end{array} \right\} (-1)^{j_{v'}+j_{w'}} \right]. \quad (8)$$

In the above equations, the index  $b$  designates core states,  $n$  designates virtual (excited) states, and  $i$  denotes an arbitrary core or excited state. In the sums over  $i$  in Eq. (6), all terms with vanishing denominators are excluded. In the sum occurring in the first term in Eq. (8), states  $i$  for which  $(iw)$  is in the model space of final states  $(v'w')$  are excluded, while in the second term, states  $i$  for which  $(iw')$  is in the model space of initial states  $(vw)$  are excluded. In the sums over  $n$  in the RPA matrix elements in Eq. (7), all core states are excluded. We denote the two-particle Coulomb + Breit interaction integrals including direct and exchange parts by  $Z_k(abcd)$  (see Eq. (2.15) in Ref. [44]).

The second-order reduced matrix element of the derivative term is given by

$$T_N^{(\text{deriv})}[vw(J) - v'w'(J')] = \alpha(E_{vw}^{(1)} - E_{v'w'}^{(1)}) P_N^{(\text{deriv})}[vw(J) - v'w'(J')], \quad (9)$$

where  $E_{vw}^{(1)}$  is the first-order correction to the energy defined by Eqs. (2.8)–(2.10) in Ref. [44], and  $\alpha$  is the fine-structure constant. The quantity  $P_N^{(\text{deriv})}$  is given by

$$P_N^{(\text{deriv})}[v_1 w_1(J) - v_2 w_2(J')] = \sqrt{[J][J']} \sum_{vw} \sum_{v'w'} \mathcal{S}^J(v_1 w_1, vw) \mathcal{S}^{J'}(v_2 w_2, v'w') \\ \times (-1)^{N+j_w+j_{v'}} \left\{ \begin{array}{ccc} J & J' & N \\ j_{v'} & j_w & j_v \end{array} \right\} Z_N^{(\text{deriv})}(v'w) \delta_{vw'}. \quad (10)$$

The expression for  $Z_N^{(\text{deriv})}(vw)$  is obtained from  $\langle v \parallel \frac{dt_N^{(1)}}{dk} \parallel w \rangle$  and given, in the case of  $N = 1$  by Eqs. (10) and (11) in Ref. [45] for electric-dipole transitions and by Eq. (9) in Ref. [46] for magnetic-dipole transitions. In Eqs. (1)–(10), we use the  $N$  subscript to describe dipole transitions with  $N =$

1, quadrupole transitions with  $N = 2$ , and octupole transitions with  $N = 3$ . Instead of using the  $N$  subscript, we use below the numbers 1, 2, and 3 to identify dipole, quadrupole, and octupole transitions as  $E1$ ,  $E2$ , and  $E3$  transitions for electric-multipole transitions and as  $M1$ ,  $M2$ , and  $M3$  transitions for magnetic-multipole transitions.

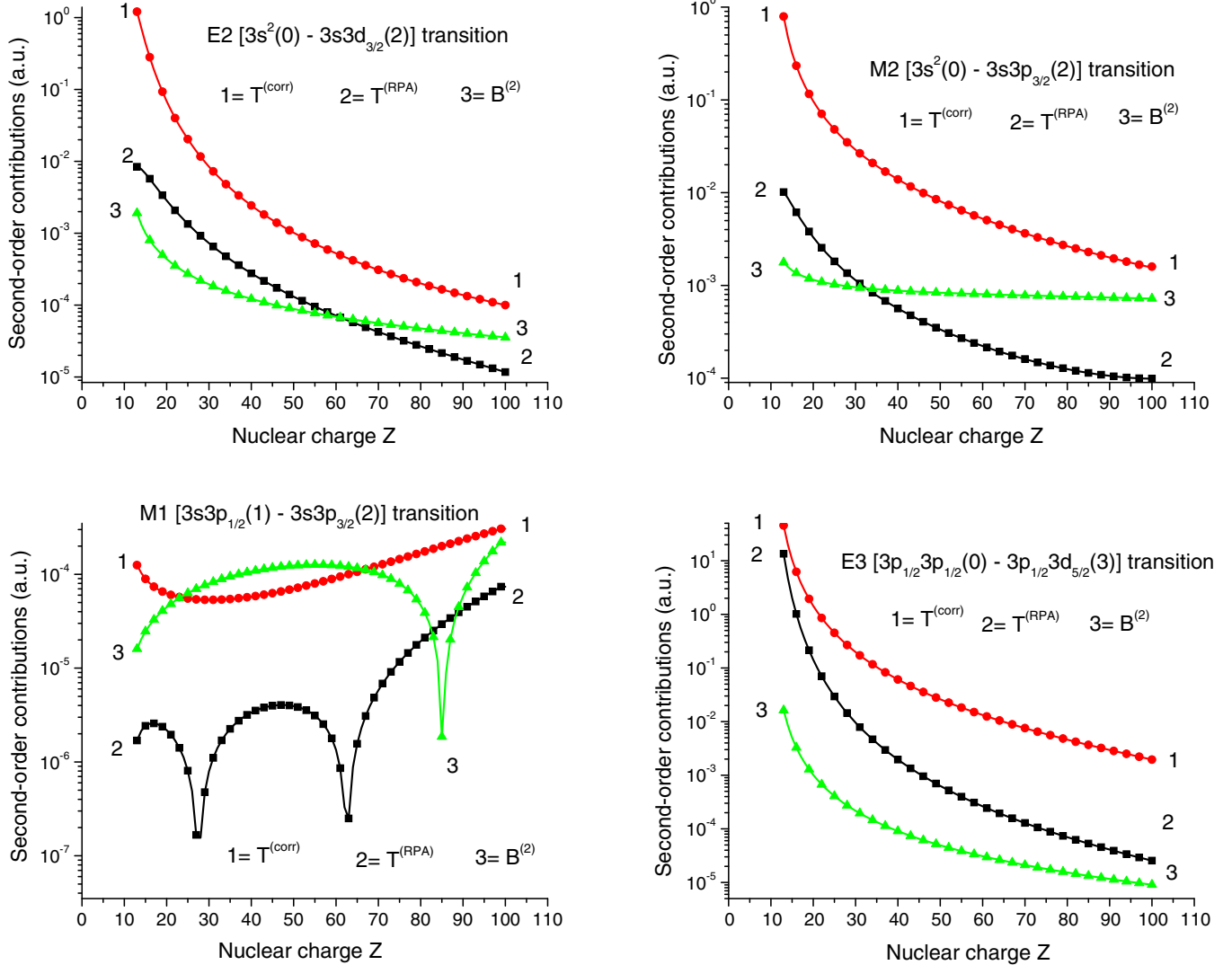
All of the second-order correlation corrections that we have discussed above result from the residual Coulomb interaction. To include correlation corrections due to the Breit interaction, the Coulomb matrix element  $X_k(abcd)$  must be modified according to the rule

$$X_k(abcd) \rightarrow X_k(abcd) + M_k(abcd) + N_k(abcd), \quad (11)$$

where  $M_k$  and  $N_k$  are magnetic radial integrals defined by Eqs. (A4) and (A5) in Ref. [47].

We consider  $M1$ ,  $M2$ , and  $E2$  transitions to evaluate the  $3s3p^3P_2$  lifetime. Specifically, we calculate the  $M1$  and  $E2$  matrix elements for the transitions between odd-parity states with  $J = 1$  and  $J = 2$  ( $[3s_{1/2}3p_j(1) + 3p_j3d_j(1)] \leftrightarrow [3s_{1/2}3p_j(2) + 3p_j3d_j(2)]$  transitions). Additionally, we evaluate the  $E2$   $[3s_{1/2}3p_j(0) + 3p_j3d_j(0)] \leftrightarrow [3s_{1/2}3p_j(2) + 3p_j3d_j(2)]$  transitions. The contribution of the  $M2$  transitions to the the  $3s3p^3P_2$  lifetime is due to the transitions between even-parity states with  $J = 0$  and odd-parity states with  $J = 2$  ( $[3s_{1/2}3s_{1/2}(0) + 3p_j3p_j(0) + 3d_j3d_j(0)] \leftrightarrow [3s_{1/2}3p_j(2) + 3p_j3d_j(2)]$  transitions).

We calculated  $E3$  matrix elements for the transitions between the 10 even-parity  $[3s_{1/2}3s_{1/2}(0) + 3p_j3p_j(0) + 3d_j3d_j(0) + 3s_{1/2}4s_{1/2}(0) + 3p_j4s_j(0) + 3d_j4d_j(0)]$  excited states and the 15  $[3p_j3d_j(3) + 3s_{1/2}4f_j(3) + 3p_j4d_j(3) + 3d_j4p_j(3) + 3d_j4f_j(3)]$  excited states to evaluate the  $3s^21S_0$  ground-state electric-octupole polarizability. In order to evaluate the  $3s^21S_0$  ground-state electric-quadrupole and electric-dipole polarizability, we use the same set of even-parity states

FIG. 1. (Color online) Second-order contributions for multipole matrix elements in Mg-like ions as a function of  $Z$ .

mentioned above and the 21 even-parity states  $[3l_j 3l'_{j'}(2) + 3l_j 4l'_{j'}(2)]$  and 18 odd-parity states  $[3l_j 3l'_{j'}(1) + 3l_j 4l'_{j'}(1)]$ , respectively.

Second-order contributions for multipole matrix elements in Mg-like ions as functions of  $Z$  are illustrated in Fig. 1. In this figure, the second-order contributions  $T^{(\text{RPA})}$ ,  $T^{(\text{corr})}$ , and  $B^{(2)}$  are shown for the  $E2$ ,  $E3$ ,  $M1$ , and  $M2$  matrix elements. We use the symbol  $B$  here to denote the Coulomb-Breit contributions to the second-order matrix elements, and  $B^{(2)} = B^{(\text{HF})} + B^{(\text{RPA})} + B^{(\text{corr})}$ . It can be seen in three panels in Fig. 1 that the largest second-order contribution is due to the correlation term,  $T^{(\text{corr})}$  [see Eq. (8)]. The RPA contribution,  $T^{(\text{RPA})}$ , is smaller than  $T^{(\text{corr})}$  by a factor of 10–30. The  $T^{(\text{RPA})}$  value becomes even less than the  $B^{(2)}$  value for the  $E2$  [ $3s^2(0)-3s3d_{3/2}(2)$ ] and  $M2$  [ $3s^2(0)-3s3p_{3/2}(2)$ ] matrix elements (see top two panels in Fig. 1). The largest value of the Coulomb-Breit contributions,  $B^{(2)}$ , occurs for the  $M1$  [ $3s3p_{1/2}(1)-3s3p_{3/2}(2)$ ] matrix element (see bottom-left panel in Fig. 1). The deep minimum in this curve around  $Z = 85$  is due to a cancellation of the  $B^{(\text{HF})}$  contribution by the sum of the  $B^{(\text{RPA})}$  and  $B^{(\text{corr})}$  contributions. It should be noted that the

values of the second-order contribution are smaller by a factor of three to four order of magnitudes than the values of the first-order contributions for the  $M1$  [ $3s3p_{1/2}(1)-3s3p_{3/2}(2)$ ] matrix element. A similar behavior of the curves describing  $T^{(\text{RPA})}$ ,  $T^{(\text{corr})}$ , and  $B^{(2)}$  is found for the other matrix elements.

It should be noted that only the  $T^{(\text{corr})}$  terms are nonzero for two-particle transitions such as the  $E2$   $3s^2(0)-3p_j3p_{j'}(2)$ ,  $M2$   $3s^2(0)-3p_j3d_{j'}(2)$ , and  $E3$   $3s^2(0)-3p_j3p_{j'}(3)$  transitions. The values of  $T^{(\text{corr})}$  terms for two-particle transitions are of the same order of magnitude as for the one-particle transitions.

#### A. $E2$ , $E3$ , $M1$ , $M2$ , and $M3$ matrix elements between physical states

The physical two-particle states are linear combinations of uncoupled two-particle states ( $vw$ ) in the model space having fixed values of angular momentum and parity; consequently, the transition amplitudes between physical states are linear combinations of the uncoupled transition matrix elements. The expansion coefficients and energies are obtained by diagonalizing the effective Hamiltonian as discussed in

TABLE I.  $E2$  and  $E3$  reduced matrix elements  $Q$  calculated in length  $L$  and velocity  $V$  forms for  $\text{Fe}^{14+}$ .

$vw(J)$	$v'w'(J')$	First order		RMBPT		$3l_13l_2{}^{1,3}L_J$	$3l_33l_4{}^{1,3}L'_{J'}$
		$L$	$V$	$L$	$V$		
Electric-quadrupole transitions							
$3s_{1/2}3p_{1/2}(0)$	$3s_{1/2}3p_{3/2}(2)$	0.347 22	0.342 93	0.367 71	0.368 01	$3s3p{}^3P_0$	$3s3p{}^3P_2$
$3s_{1/2}3p_{1/2}(0)$	$3p_{1/2}3d_{3/2}(2)$	0.319 03	0.319 61	0.356 94	0.357 36	$3s3p{}^3P_0$	$3p3d{}^3F_2$
$3s_{1/2}3p_{1/2}(0)$	$3p_{1/2}3d_{5/2}(2)$	-0.169 94	-0.159 43	-0.184 58	-0.184 71	$3s3p{}^3P_0$	$3p3d{}^1D_2$
$3s_{1/2}3p_{1/2}(0)$	$3p_{3/2}3d_{3/2}(2)$	-0.278 28	-0.294 06	-0.267 47	-0.268 64	$3s3p{}^3P_0$	$3p3d{}^3P_2$
$3p_{3/2}3d_{3/2}(0)$	$3p_{3/2}3d_{3/2}(2)$	0.134 11	-0.034 29	0.614 34	0.617 76	$3p3d{}^3P_0$	$3p3d{}^3P_2$
$3s_{1/2}3p_{1/2}(1)$	$3s_{1/2}3p_{3/2}(2)$	0.520 12	0.371 99	0.580 17	0.582 80	$3s3p{}^3P_1$	$3s3p{}^3P_2$
$3s_{1/2}3p_{1/2}(1)$	$3p_{1/2}3d_{5/2}(2)$	0.019 75	0.011 54	0.030 06	0.030 07	$3s3p{}^3P_1$	$3p3d{}^1D_2$
$3s_{1/2}3p_{1/2}(1)$	$3p_{3/2}3d_{3/2}(2)$	-0.310 52	-0.318 66	-0.303 34	-0.304 80	$3s3p{}^3P_1$	$3p3d{}^3P_2$
$3s_{1/2}3p_{3/2}(1)$	$3p_{1/2}3d_{3/2}(2)$	-0.164 94	-0.142 40	-0.199 12	-0.198 41	$3s3p{}^1P_1$	$3p3d{}^3F_2$
$3s_{1/2}3p_{3/2}(1)$	$3p_{1/2}3d_{5/2}(2)$	-0.498 48	-0.465 33	-0.601 95	-0.602 34	$3s3p{}^1P_1$	$3p3d{}^1D_2$
$3p_{1/2}3d_{3/2}(1)$	$3p_{3/2}3d_{5/2}(2)$	0.312 86	0.121 75	0.566 59	0.567 09	$3p3d{}^3P_1$	$3p3d{}^3D_2$
$3p_{3/2}3d_{3/2}(1)$	$3s_{1/2}3p_{3/2}(2)$	-0.334 81	-0.344 66	-0.323 40	-0.324 49	$3p3d{}^3D_1$	$3s3p{}^3P_2$
Electric-octupole transitions							
$3s_{1/2}3s_{1/2}(0)$	$3p_{1/2}3d_{5/2}(3)$	0.004 66	0.004 70	0.011 61	0.011 65	$3s^2{}^1S_0$	$3p3d{}^3F_3$
$3s_{1/2}3s_{1/2}(0)$	$3p_{3/2}3d_{3/2}(3)$	-0.004 73	-0.004 78	-0.011 95	-0.012 01	$3s^2{}^1S_0$	$3p3d{}^3D_3$
$3s_{1/2}3s_{1/2}(0)$	$3p_{3/2}3d_{5/2}(3)$	0.063 58	0.064 47	0.158 22	0.159 32	$3s^2{}^1S_0$	$3p3d{}^1F_3$
$3p_{1/2}3p_{1/2}(0)$	$3p_{1/2}3d_{5/2}(3)$	-0.320 30	-0.324 64	-0.417 61	-0.418 53	$3p^2{}^3P_0$	$3p3d{}^3F_3$
$3p_{1/2}3p_{1/2}(0)$	$3p_{3/2}3d_{3/2}(3)$	0.165 92	0.168 17	0.156 91	0.157 10	$3p^2{}^3P_0$	$3p3d{}^3D_3$
$3p_{3/2}3p_{3/2}(0)$	$3p_{1/2}3d_{5/2}(3)$	0.040 18	0.040 82	0.226 17	0.226 68	$3p^2{}^1S_0$	$3p3d{}^3F_3$
$3p_{3/2}3p_{3/2}(0)$	$3p_{3/2}3d_{3/2}(3)$	-0.009 59	-0.009 79	-0.029 75	-0.029 87	$3p^2{}^1S_0$	$3p3d{}^3D_3$
$3d_{3/2}3d_{3/2}(0)$	$3p_{1/2}3d_{5/2}(3)$	-0.227 61	-0.230 77	-0.190 79	-0.191 12	$3d^2{}^3P_0$	$3p3d{}^3F_3$
$3d_{3/2}3d_{3/2}(0)$	$3p_{3/2}3d_{5/2}(3)$	0.012 01	0.012 21	0.027 67	0.027 70	$3d^2{}^3P_0$	$3p3d{}^1F_3$
$3d_{5/2}3d_{5/2}(0)$	$3p_{1/2}3d_{5/2}(3)$	-0.020 57	-0.020 74	-0.018 33	-0.018 34	$3d^2{}^1S_0$	$3p3d{}^3F_3$
$3d_{5/2}3d_{5/2}(0)$	$3p_{3/2}3d_{3/2}(3)$	0.015 60	0.015 73	0.018 05	0.018 10	$3d^2{}^1S_0$	$3p3d{}^3D_3$

Refs. [33,44–46,49–52]. The first-order expansion coefficient  $C_1^\lambda(vw)$  is the  $\lambda$ th eigenvector of the first-order effective Hamiltonian, and  $E_1^\lambda$  is the corresponding eigenvalue.

The transition matrix element between the initial eigenstate  $I$  with angular momentum  $J$  and the final state  $F$  with angular momentum  $J'$  is given by

$$\begin{aligned} Q_N^{(1+2)}(I - F) &= \frac{1}{E_N^I - E_N^F} \sum_{vw} \sum_{v'w'} C_1^I(vw) C_1^F(v'w') \\ &\times ([\varepsilon_{vw} - \varepsilon_{v'w'}] \{TB_N^{(1+2)}[vw(J) - v'w'(J')]\} \\ &+ [E_1^I - E_1^F - \varepsilon_{vw} + \varepsilon_{v'w'}] P_N^{(\text{der})}[vw(J) - v'w'(J')]). \end{aligned} \quad (12)$$

Here,  $\varepsilon_{vw} = \varepsilon_v + \varepsilon_w$  and  $TB_N^{(1+2)} = T_N^{(1)} + T_N^{(\text{DF})} + T_N^{(\text{RPA})} + T_N^{(\text{corr})} + B_N^{(\text{DF})} + B_N^{(\text{RPA})} + B_N^{(\text{corr})}$ . The mixing coefficients  $C_1^I(vw)$  and  $C_1^F(v'w')$  and energies  $E_N^I$  and  $E_N^F$  are obtained by diagonalizing the first-order effective Hamiltonian, which includes both Coulomb and Breit interactions [33]. The energy terms  $E_N^I$  and  $E_N^F$  are defined as the sum of the DF energies  $E^{(0)}$  and the first-order energies  $E^{(1)}$  obtained after diagonalization [33] of the initial  $I$  and final  $F$  states:  $E_N = E^{(0)} + NE^{(1)}$ . Using these formulas together with the above-discussed reduced matrix elements, we transform these matrix element basic states to matrix elements between physical states.

The values of  $E2$  and  $E3$  reduced matrix elements in length and velocity forms are listed in Table I. Although we use an intermediate-coupling scheme, it is nevertheless convenient to label the physical states using  $jj$  labeling for high  $Z$  and  $LS$  labeling for low  $Z$ ; both designations are used in Table I. The third and fourth columns in Table I show  $L$  and  $V$  values of reduced matrix elements calculated in first-order RMBPT. The  $L - V$  difference is about 5%–10% for most cases, except the  $3p_{3/2}3d_{3/2}(0)-3p_{3/2}3d_{3/2}(2)$  and  $3p_{1/2}3d_{3/2}(1)-3p_{3/2}3d_{5/2}(2)$  transitions. Including the second-order contributions (“RMBPT” columns in Table I) decreases the  $L - V$  difference to 0.2%–2%. This nonzero  $L - V$  difference arises because we start our RMBPT calculations using a nonlocal DF potential. If we were to replace the DF potential with a local potential, the differences would disappear completely. It should be emphasized that we include the negative-energy-state contributions to the sums over the intermediate states (see Refs. [53] and [54] for details). Neglecting the negative-energy-state contributions leads to only small changes in the  $L$ -form matrix elements but to substantial changes in some of the  $V$ -form matrix elements, with a consequent loss of gauge independence.

In Fig. 2, we illustrate the  $Z$  dependence of the line strengths ( $S$ ) of  $E2$ ,  $M1$ , and  $M2$  transitions from the  $3s3p{}^3P_0$ ,  $3s3p{}^3P_1$ , and  $3s^2{}^1S_0$  levels to the  $3s3p{}^3P_2$  excited levels in the Mg-like sequence. Those line strengths are obtained as a square of matrix elements given by Eq. (13). We can see in Fig. 2 that the largest value of the line strengths is for the  $3s^2{}^1S_0-3s3p{}^3P_2$

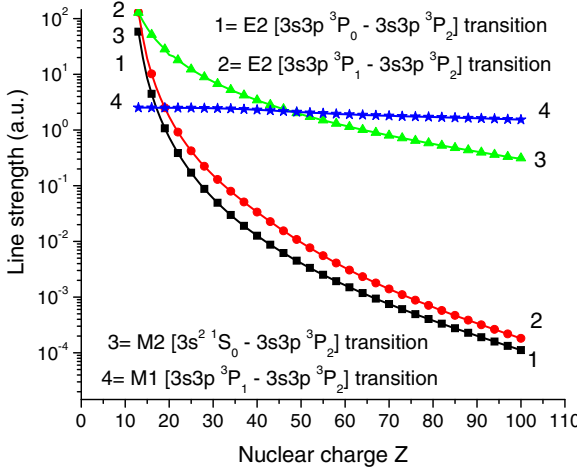


FIG. 2. (Color online) Line strengths for  $E2$ ,  $M1$ , and  $M2$  transitions in Mg-like ions as a function of  $Z$ .

$M2$  transition for small- $Z$  ions, from  $Z = 14$  up to  $Z = 47$ . For high- $Z$  ions, the largest value of the line strengths is for the  $3s3p^3P_1-3s3p^3P_2$   $M1$  transition. It should be noted that the value of the  $M1$   $3s3p^3P_1-3s3p^3P_2$  line strength is almost constant for the entire interval of  $Z$ , decreasing slowly from  $S = 2.51$  a.u. for  $Z = 13$  up to  $S = 1.53$  a.u. for  $Z = 100$ . The value of the  $M2$   $3s^2^1S_0-3s3p^3P_2$  line strengths changes by a factor of 400, from  $S = 128$  a.u. for  $Z = 13$  up to  $S = 0.314$  a.u. for  $Z = 100$ . The smallest values of the line strength shown in Fig. 2 are for the  $3s3p^3P_0-3s3p^3P_2$  and  $3s3p^3P_1-3s3p^3P_2$   $E2$  transitions. The value of these transitions decreases by almost five orders of magnitude in the interval  $Z = 14-100$ .

The nonrelativistic limit of the magnetic-dipole matrix element given by Eq. (5) was investigated by Safronova *et al.* [46]. It was shown that in the case of  $n_v = n_w$ , the value of  $T_1(v, w)$  is independent of  $Z$ . The leading term for the line strength of the  $M2$  transitions was found in [49] to be proportional to  $\sim 1/Z^2$ . Following the procedure given in [49], we find that the leading term for the line strengths of  $E2$  transitions is proportional to  $\sim 1/Z^4$ .

### III. MULTIPOLE CONTRIBUTIONS TO THE LIFETIME OF THE $3s3p^3P_2$ LEVEL IN Mg-LIKE IONS

The  $E2$ ,  $M1$ , and  $M2$  transition probabilities  $A_r$  ( $s^{-1}$ ) for the transitions from the  $3s3p^3P_0$ ,  $3s3p^3P_1$ , and  $3s^2^1S_0$  states to the  $3s3p^3P_2$  excited states are obtained in terms of line strengths  $S$  (a.u.) and wavelength  $\lambda$  ( $\text{\AA}$ ) as

$$\begin{aligned} A_r(E2) &= \frac{1.119\,95 \times 10^{18}}{(2J+1)\lambda^5} S^{(E2)}, \\ A_r(M2) &= \frac{1.490\,97 \times 10^{13}}{(2J+1)\lambda^5} S^{(M2)}, \\ A_r(M1) &= \frac{2.697\,35 \times 10^{13}}{(2J+1)\lambda^3} S^{(M1)}. \end{aligned} \quad (13)$$

The values of the  $S^{(E2)}$ ,  $S^{(M2)}$ , and  $S^{(M1)}$  line strengths are illustrated in Fig. 2. We use available recommended NIST

energies [48] and RMBPT energies obtained by Safronova *et al.* [33] to evaluate the multipole transition rates in Eq. (13) for Mg-like ions with  $Z = 13-100$ . In Table II, we present a limited set of our results to compare with the available theoretical values. Transition rates  $A_r$  for the  $E2$ ,  $M1$ , and  $M2$  transitions in Mg-like ions are evaluated in first-order (RMBPT-I) and second-order (RMBPT) RMBPT. The RMBPT energies are compared with NIST energies [48] in columns 2 and 3 in Table II. The energies for Mg-like Ag and Yb given in the column “NIST” are from Ref. [29]. Our results for transition rates, listed in columns “RMBPT-1” and “RMBPT” in Table II, are compared with the transition rates calculated by the GRASP2K code [29,30] and by the GRASP code [31]. It is evident in Table II that the transition rates calculated by the GRASP2K code [29,30] or the GRASP code [31] are in better agreement with our RMBPT-1 results than with the results given in the RMBPT columns in Table II. The differences between our RMBPT-1 values and the GRASP2K values [29] are less than 1% for the  $3s^2^1S_0-3s3p^3P_2$   $M2$  and  $3s3p^3P_1-3s3p^3P_2$   $M1$  transitions and about 1%-3% for the  $3s3p^3P_1-3s3p^3P_2$  and  $3s3p^3P_0-3s3p^3P_2$   $E2$  transitions. There is a larger difference for ions with a small degree of ionization, i.e.,  $\text{Al}^+$  and  $\text{Si}^{2+}$ . Excellent agreement is found between our first-order RMBPT-1 and the GRASP2K values from Ref. [30]. The difference is about 1%-2% for the  $M2$   $3s^2^1S_0-3s3p^3P_2$  transition and 0.2%-1% for the  $M1$   $3s3p^3P_1-3s3p^3P_2$  transition. Even for  $\text{Al}^+$  and  $\text{Si}^{2+}$  ions, the disagreement is 3% and 6% for the  $M2$   $3s^2^1S_0-3s3p^3P_2$  transition and 3% and 1% for the  $M1$   $3s3p^3P_1-3s3p^3P_2$  transition. In Table II, we compare transition rates calculated by the RMBPT code and by the GRASP code [31] for  $\text{Fe}^{14+}$ ,  $\text{Co}^{15+}$ , and  $\text{Ni}^{16+}$  ions. Excellent agreement is found between our first-order RMBPT results and the GRASP results. The difference is less than 0.1% for the the  $3s^2^1S_0-3s3p^3P_2$   $M2$  transition, less than 1% for the  $3s3p^3P_1-3s3p^3P_2$   $E2$  transition, and less than 3% for the  $3s3p^3P_1-3s3p^3P_2$   $M1$  and  $3s3p^3P_0-3s3p^3P_2$   $E2$  transitions.

The  $Z$  dependencies of these  $M2$ ,  $M1$ , and  $E2$  transition rates are shown in Fig. 3. The largest values among these transitions are found for the  $3s^2^1S_0-3s3p^3P_2$   $M2$  transition for small  $Z = 13-20$ . With increasing  $Z$ , the transition rate of this transition decreases and becomes smaller at  $Z = 45$  than the  $3s3p^3P_1-3s3p^3P_2$  and  $3s3p^3P_0-3s3p^3P_2$   $E2$  transitions. The largest value of the transition rates for high- $Z$  ions ( $Z = 21-100$ ) is for the  $3s3p^3P_1-3s3p^3P_2$   $M1$  transition. For example, the branching ratio of the  $E2$ ,  $M2$ , and  $M1$  transition is equal to  $0.56 \times 10^{-4}$ , 0.52, and 0.48 for  $Z = 20$ ,  $0.32 \times 10^{-2}$ ,  $0.21 \times 10^{-2}$  and 0.99 for  $Z = 42$ , and  $0.084$ ,  $0.002$ , and 0.91 for  $Z = 92$ , respectively.

The lifetime of the  $3s3p^3P_2$  level is defined by the sum of the transition rates of four  $E2$ ,  $M1$ , and  $E2$  transitions:  $A^{E2}(3s3p^3P_1-3s3p^3P_2)$ ,  $A^{E2}(3s3p^3P_0-3s3p^3P_2)$ ,  $A^{M1}(3s3p^3P_1-3s3p^3P_2)$ , and  $A^{M2}(3s^2^1S_0-3s3p^3P_2)$ . Tabulated data for the lifetime of the  $3s3p^3P_2$  level are listed for Mg-like ions with  $Z = 13-100$  in Table III. The RMBPT-1 and RMBPT lifetimes are compared with the GRASP2K results presented in Refs. [29] and [30]. There are no large differences (0.05%-0.8%) in the RMBPT-1 and RMBPT lifetimes for high- $Z$  ions, with  $Z = 24-100$ . The largest contribution of the second-order terms is for  $\text{Al}^+$  and  $\text{Si}^{2+}$

TABLE II. Energies ( $E$ ; in  $\text{cm}^{-1}$ ) and transition rates ( $A_r$ ; in  $\text{s}^{-1}$ ) for  $E2$ ,  $M1$ , and  $M2$  transitions in Mg-like ions evaluated in first-order (RMBPT-I) and second-order (RMBPT) RMBPT.  $A[B]$  means  $A \times 10^B$ . Our results are compared with the GRASP2K results [29,30]<sup>a</sup> and GRASP results [31]<sup>b</sup>.

Z	Energy ( $\text{cm}^{-1}$ )		Transition rate ( $\text{s}^{-1}$ )		Transition rate ( $\text{s}^{-1}$ )		Energy ( $\text{cm}^{-1}$ )		Transition rate ( $\text{s}^{-1}$ )		
	RMBPT	NIST [48]	RMBPT-1	RMBPT	Theory [30]	Theory	RMBPT	NIST [48]	RMBPT-1	RMBPT	Theory
<i>M2</i> [ $3s^2 \text{ } ^1\text{S}_0 - 3s3p \text{ } ^3\text{P}_2$ ] transition						<i>E2</i> [ $3s3p \text{ } ^3\text{P}_0 - 3s3p \text{ } ^3\text{P}_2$ ] transition					
13	37 943	37 578	3.297[-3]	3.002[-3]	3.41[-3]	3.551[-3] <sup>a</sup>	186	185	1.516[-10]	2.896[-10]	1.951[-11] <sup>a</sup>
14	53 103	53 115	1.187[-2]	1.137[-2]	1.26[-2]	1.246[-2] <sup>a</sup>	392	390	2.574[-9]	4.131[-9]	3.084[-9] <sup>a</sup>
15	68 702	68 615	3.121[-2]	3.077[-2]	3.25[-2]		700	697	2.305[-8]	3.190[-8]	
16	83 951	84 155	6.485[-2]	6.401[-2]	6.83[-2]		1135	1131	1.435[-7]	1.885[-7]	
17	99 738	99 782	1.213[-1]	1.222[-1]	1.26[-1]		1725	1720	7.029[-7]	8.903[-7]	
18	115 587	115 590	2.058[-1]	2.091[-1]		1.992[-1] <sup>a</sup>	2499	2489	2.881[-6]	3.552[-6]	2.993[-6] <sup>a</sup>
19	131 680	131 582	3.271[-1]	3.335[-1]	3.36[-1]		3493	3485	1.035[-5]	1.250[-5]	
20	147 890	147 912	5.137[-1]	4.915[-1]	5.06[-1]	4.902[-1] <sup>a</sup>	4742	4734	3.339[-5]	3.965[-5]	3.412[-5] <sup>a</sup>
21	164 237	164 451	7.107[-1]	7.448[-1]	7.33[-1]		6286	6274	9.860[-5]	1.155[-4]	
22	181 285	181 371	1.007[0]	1.052[0]	1.03[0]		8166	8155	2.701[-4]	3.127[-4]	
23	198 681	198 737	1.389[0]	1.453[0]	1.42[0]		10 430	10 426	6.945[-4]	7.964[-4]	
24	216 531	216 557	1.881[0]	1.969[0]	1.92[0]		13 124	13 113	1.689[-3]	1.920[-3]	
25	234 900	234 905	2.507[0]	2.627[0]	2.56[0]		16 300	16 301	3.910[-3]	4.414[-3]	
26	253 853	253 820	3.299[0]	3.460[0]	3.36[0]	3.299[0] <sup>b</sup>	20 014	19 978	8.672[-3]	9.725[-3]	8.861[-3] <sup>b</sup>
27	273 454	273 414	4.298[0]	4.510[0]	4.37[0]	4.300[0] <sup>b</sup>	24 324	24 333	1.850[-2]	2.063[-2]	1.891[-2] <sup>b</sup>
28	293 769	293 686	5.553[0]	5.829[0]	5.64[0]	5.557[0] <sup>b</sup>	29 290	29 255	3.812[-2]	4.229[-2]	3.896[-2] <sup>b</sup>
29	314 866	314 753	7.125[0]	7.481[0]	7.23[0]	7.066[0] <sup>a</sup>	34 975	34 937	7.608[-2]	8.400[-2]	7.839[-2] <sup>a</sup>
30	336 821	336 699	9.093[0]	9.547[0]	9.22[0]		41 451	41 451	1.476[-1]	1.622[-1]	
31	359 708	359 566	1.155[1]	1.213[1]	1.17[1]		48 788	48 751	2.787[-1]	3.053[-1]	
35	462 237	462 162	2.926[1]	3.067[1]		2.906[1] <sup>a</sup>	88 304	88 639	2.836[0]	3.068[0]	2.924[0] <sup>a</sup>
47	930 405	929 728	4.505[2]	4.676[2]		4.497[2] <sup>a</sup>	356 996	356 448	6.820[2]	7.207[2]	6.996[2] <sup>a</sup>
70	3320 482	3319 340	9.471[4]	9.625[4]		9.487[4] <sup>a</sup>	2288 881	2286 899	1.020[6]	1.056[6]	1.039[6] <sup>a</sup>
<i>M1</i> [ $3s3p \text{ } ^3\text{P}_1 - 3s3p \text{ } ^3\text{P}_2$ ] transition						<i>E2</i> [ $3s3p \text{ } ^3\text{P}_1 - 3s3p \text{ } ^3\text{P}_2$ ] transition					
13	125	124	2.634[-5]	2.646[-5]	2.56[-5]	2.520[-5] <sup>a</sup>	125	124	4.681[-11]	8.903[-11]	5.818[-11] <sup>a</sup>
14	263	262	2.453[-4]	2.475[-4]	2.42[-4]	2.328[-4] <sup>a</sup>	263	262	7.882[-10]	1.278[-9]	9.239[-10] <sup>a</sup>
15	471	469	1.409[-3]	1.424[-3]	1.39[-3]		471	469	7.160[-9]	9.917[-9]	
16	765	762	6.036[-3]	6.074[-3]	5.96[-3]		765	762	4.498[-8]	5.983[-8]	
17	1166	1161	2.137[-2]	2.146[-2]	2.11[-2]		1166	1161	2.235[-7]	2.884[-7]	
18	1694	1685	6.552[-2]	6.573[-2]	1	6.428[-2] <sup>a</sup>	1694	1685	9.290[-7]	1.175[-6]	9.665[-7] <sup>a</sup>
19	2377	2373	1.810[-1]	1.814[-1]	1.80[-1]		2377	2373	3.404[-6]	4.245[-6]	
20	3240	3237	4.581[-1]	4.590[-1]	4.57[-1]	4.571[-1] <sup>a</sup>	3240	3237	1.120[-5]	1.385[-5]	1.146[-5] <sup>a</sup>
21	4315	4310	1.082[0]	1.083[0]	1.08[0]		4315	4310	3.385[-5]	4.166[-5]	
22	5635	5624	2.407[0]	2.410[0]	2.39[0]		5635	5624	9.514[-5]	1.169[-4]	
23	7237	7228	5.095[0]	5.100[0]	5.07[0]		7237	7228	2.514[-4]	3.089[-4]	
24	9164	9158	1.033[1]	1.034[1]	1.03[1]		9164	9158	6.304[-4]	7.767[-4]	
25	11458	11467	2.017[1]	2.019[1]	2.02[1]		11458	11467	1.508[-3]	1.866[-3]	
26	14171	14160	3.810[1]	3.812[1]	3.80[1]	3.704[1] <sup>b</sup>	14171	14160	3.463[-3]	4.309[-3]	3.483[-3] <sup>b</sup>
27	17355	17354	6.985[1]	6.985[1]	6.98[1]	6.796[1] <sup>b</sup>	17355	17354	7.665[-3]	9.601[-3]	7.701[-3] <sup>b</sup>
28	21069	21152	1.247[2]	1.247[2]	1.242[2]	1.214[2] <sup>b</sup>	21069	21152	1.641[-2]	2.072[-2]	1.647[-2] <sup>b</sup>
29	25374	25352	2.171[2]	2.172[2]	2.162[2]	2.156[2] <sup>a</sup>	25374	25352	3.410[-2]	4.338[-2]	3.552[-3] <sup>a</sup>
30	30341	30338	3.700[2]	3.701[2]	3.692[2]		30341	30338	6.894[-2]	8.845[-2]	
31	36042	36047	6.178[2]	6.180[2]	6.167[2]		36042	36047	1.359[-1]	1.758[-1]	
35	67830	67961	4.032[3]	4.032[3]		4.013[3] <sup>a</sup>	67830	67961	1.648[0]	2.197[0]	1.690[0] <sup>a</sup>
47	305967	305411	3.325[5]	3.325[5]		3.306[5] <sup>a</sup>	305967	305411	6.193[2]	8.226[2]	6.308[2] <sup>a</sup>
70	2174141	2172015	9.964[7]	9.965[7]		9.937[7] <sup>a</sup>	2174141	2172015	1.323[6]	1.522[6]	1.342[6] <sup>a</sup>

(9% and 4%). This second-order contribution is much less (1.3%) already for three times ionized Mg-like  $\text{P}^{3+}$ . Similar contributions (0.7%–2.2%) are found for Mg-like ions with  $Z = 16$ –23.

The lifetimes of the  $3s3p \text{ } ^3\text{P}_2$  level in Mg-like  $\text{Co}^{15+}$  ( $13.6 \pm 1.8$  ms) and  $\text{Ni}^{16+}$  ( $7.672 \pm 0.015$  ms) were recently measured by Träbert *et al.* [28]. The values of our RMBPT-1 and RMBPT lifetimes for Mg-like  $\text{Co}^{15+}$

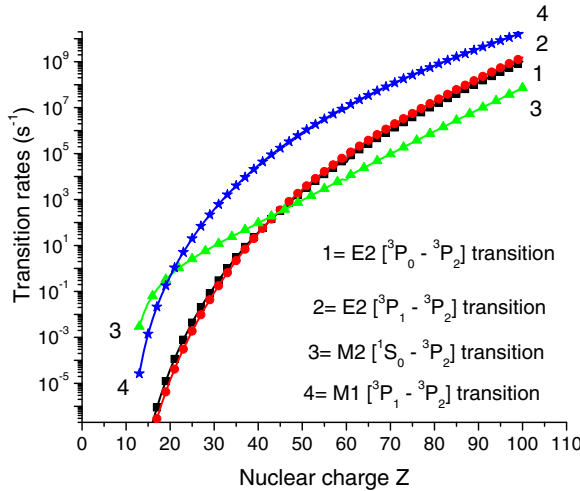


FIG. 3. (Color online) Transition rates for the lifetime of the  $3s3p\ ^3P_2$  level in Mg-like ions as a function of  $Z$ .

(13.48 and 13.44 ms) and  $\text{Ni}^{16+}$  (7.674–7.657 ms) are in excellent agreement with their experimental results. Unfortunately, we cannot compare our results for Mg-like

TABLE III. Lifetime (in s) of  $3s3p\ ^3P_2$  level in Mg-like ions evaluated in first-order (RMBPT-I) and second-order (RMBPT) RMBPT.  $A[B]$  means  $A \times 10^B$ . Our results are compared with the GRASP2K results presented in Ref. [30]<sup>a</sup> and Ref. [29]<sup>b</sup>.

$Z$	RMBPT-1	RMBPT	Theory	Theory	$Z$	RMBPT-1	RMBPT	Theory	$Z$	RMBPT-1	RMBPT	Theory
13	3.01[2]	3.30[2]	2.91[2] <sup>a</sup>	2.796[2] <sup>b</sup>	42	1.57[-5]	1.57[-5]		71	7.99[-9]	7.97[-9]	7.985[-9] <sup>b</sup>
14	8.25[1]	8.61[1]	7.78[1] <sup>a</sup>	7.878[1] <sup>b</sup>	43	1.11[-5]	1.11[-5]		72	6.53[-9]	6.52[-9]	
15	3.07[1]	3.11[1]	2.95[1] <sup>a</sup>		44	7.89[-6]	7.88[-6]		73	5.36[-9]	5.34[-9]	
16	1.41[1]	1.43[1]	1.35[1] <sup>a</sup>		45	5.66[-6]	5.66[-6]		74	4.40[-9]	4.39[-9]	
17	7.01[0]	6.96[0]	6.81[0] <sup>a</sup>		46	4.10[-6]	4.10[-6]		75	3.63[-9]	3.62[-9]	
18	3.69[0]	3.64[0]		3.795[0] <sup>b</sup>	47	2.99[-6]	2.99[-6]	3.009[-6] <sup>b</sup>	76	3.00[-9]	2.99[-9]	
19	1.97[0]	1.94[0]	1.94[0] <sup>a</sup>		48	2.20[-6]	2.20[-6]		77	2.48[-9]	2.47[-9]	
20	1.03[0]	1.05[0]	1.04[0] <sup>a</sup>	1.056[0] <sup>b</sup>	49	1.63[-6]	1.63[-6]		78	2.05[-9]	2.05[-9]	2.053[-9] <sup>b</sup>
21	5.58[-1]	5.47[-1]	5.52[-1] <sup>a</sup>		50	1.22[-6]	1.21[-6]		79	1.71[-9]	1.70[-9]	
22	2.93[-1]	2.89[-1]	2.92[-1] <sup>a</sup>		51	9.13[-7]	9.12[-7]		80	1.42[-9]	1.41[-9]	
23	1.54[-1]	1.53[-1]	1.54[-1] <sup>a</sup>		52	6.90[-7]	6.89[-7]		81	1.18[-9]	1.18[-9]	
24	8.19[-2]	8.12[-2]	8.18[-2] <sup>a</sup>		53	5.24[-7]	5.24[-7]	5.278[-7] <sup>b</sup>	82	9.88[-10]	9.84[-10]	
25	4.41[-2]	4.38[-2]	4.39[-2] <sup>a</sup>		54	4.01[-7]	4.00[-7]		83	8.26[-10]	8.23[-10]	
26	2.41[-2]	2.40[-2]	2.42[-2] <sup>a</sup>	2.437[-2] <sup>b</sup>	55	3.08[-7]	3.07[-7]		84	6.92[-10]	6.89[-10]	
27	1.35[-2]	1.34[-2]	1.35[-2] <sup>a</sup>		56	2.38[-7]	2.37[-7]		85	5.80[-10]	5.78[-10]	
28	7.67[-3]	7.66[-3]	7.70[-3] <sup>a</sup>		57	1.85[-7]	1.84[-7]		86	4.88[-10]	4.86[-10]	
29	4.46[-3]	4.45[-3]	4.48[-3] <sup>a</sup>	4.489[-3] <sup>b</sup>	58	1.44[-7]	1.44[-7]		87	4.10[-10]	4.09[-10]	
30	2.64[-3]	2.63[-3]	2.64[-3] <sup>a</sup>	2.658[-3] <sup>b</sup>	59	1.13[-7]	1.13[-7]	1.131[-7] <sup>b</sup>	88	3.46[-10]	3.44[-10]	
31	1.59[-3]	1.59[-3]			60	1.14[-7]	1.13[-7]		89	2.92[-10]	2.90[-10]	
32	9.72[-4]	9.72[-4]			61	7.00[-8]	6.99[-8]		90	2.46[-10]	2.45[-10]	
33	6.06[-4]	6.05[-4]			62	5.55[-8]	5.54[-8]		91	2.08[-10]	2.07[-10]	
34	3.83[-4]	3.83[-4]			63	4.42[-8]	4.41[-8]		92	1.76[-10]	1.75[-10]	
35	2.46[-4]	2.46[-4]	2.471[-4] <sup>b</sup>		64	3.53[-8]	3.52[-8]	3.538[-8] <sup>b</sup>	93	1.49[-10]	1.48[-10]	
36	1.60[-4]	1.60[-4]			65	2.83[-8]	2.82[-8]		94	1.27[-10]	1.26[-10]	
37	1.06[-4]	1.06[-4]			66	2.27[-8]	2.27[-8]		95	1.07[-10]	1.07[-10]	
38	7.05[-5]	7.05[-5]			67	1.83[-8]	1.83[-8]		96	9.13[-11]	9.08[-11]	
39	4.77[-5]	4.76[-5]			68	1.48[-8]	1.48[-8]		97	7.76[-11]	7.72[-11]	
40	3.26[-5]	3.26[-5]			69	1.20[-8]	1.20[-8]		98	6.61[-11]	6.57[-11]	
41	2.25[-5]	2.25[-5]			70	9.80[-9]	9.77[-9]	9.819[-9] <sup>b</sup>	99	5.63[-11]	5.59[-11]	
									100	4.79[-11]	4.76[-11]	

$\text{Cu}^{17+}$  since the results in [28] are with the inclusion of hyperfine mixing, which was not considering in the present work.

#### IV. MULTPOLE GROUND-STATE STATIC POLARIZABILITIES IN Mg-LIKE IONS

The  $N$ -pole ground-state static polarizability  $\alpha_0$  of level  $|aJ\rangle$  is defined as [55]

$$\alpha_0^{(N)}(aJ) = \frac{2}{(2N+1)(2J+1)} \sum_n \frac{|\langle aJ \| D \| nJ' \rangle|^2}{E(aJ) - E(nJ')}. \quad (14)$$

Here,  $\langle aJ \| D \| nJ' \rangle$  is the coupled electric- $N$ -pole matrix element defined by Eq. (13) and  $E(aJ)$  is the eigenvalue of the level  $|aJ\rangle$ . In the case of the  $3s^2\ ^1S_0$  ground state of Mg-like ions, we can rewrite Eq. (14) as

$$\begin{aligned} & \alpha_0^{(N)}(3s^2\ ^1S_0) \\ &= \frac{2}{(2N+1)} \sum_n \sum_{l,l'} \frac{|\langle 3s^2\ ^1S_0 \| D \| 3l'l\ ^{1,3}L_N \rangle|^2}{E(3s^2\ ^1S_0) - E(3l'l\ ^{1,3}L_N)}, \end{aligned} \quad (15)$$

TABLE IV. Contributions to the electric-dipole polarizability of Mg-like ions in the  $3s^2 \text{ } ^1S_0$  ground state. Designations:  $\Delta E = E(3s^2 \text{ } ^1S_0) - E(3l'nl^{(1,3)}L_1)$ ,  $D = \langle 3s^2 \text{ } ^1S_0 | D | 3l'nl^{(1,3)}L_1 \rangle$ ,  $I = I(3l'nl^{(1,3)}L_1) = \frac{2}{3} \frac{|\langle 3s^2 \text{ } ^1S_0 | D | 3l'nl^{(1,3)}L_1 \rangle|^2}{E(3s^2 \text{ } ^1S_0) - E(3l'nl^{(1,3)}L_1)}$ ,  $\alpha_0(3s^2 \text{ } ^1S_0, n) = \sum_{l,l'} I(3l'nl^{(1,3)}L_1)$ . All values are in a.u. Excitation energies (in cm<sup>-1</sup>) and absolute values of the corresponding reduced electric-dipole matrix elements are listed in columns “ $\Delta E$ ” and “ $D$ .”  $I$  values are calculated with NIST energies [48] or with RMBPT energies when NIST energies are absent. Contributions from the core and  $vc$  terms are listed in rows “ $\alpha_c$ ” and “ $\alpha_{vc}$ .” Final polarizability values are listed in “total” rows.  $A[B]$  means  $A \times 10^B$ .

Level	$\Delta E$ (cm <sup>-1</sup> )	$D$ (a.u.)	$I$ ( $a_0^3$ )	$\Delta E$ (cm <sup>-1</sup> )	$D$ (a.u.)	$I$ ( $a_0^3$ )	$\Delta E$ (cm <sup>-1</sup> )	$D$ (a.u.)	$I$ ( $a_0^3$ )
Mg-like Si <sup>2+</sup>									
$3s3p \text{ } ^3P_1$	52 853	0.0100	2.757[-4]	239 660	0.0641	2.508[-3]	412 290	-0.1150	4.696[-3]
$3s3p \text{ } ^1P_1$	82 884	2.5440	1.142[1]	351 911	-0.8603	3.077[-1]	632 187	-0.5530	7.078[-2]
$3s4p \text{ } ^1P_1$	176 487	-0.0091	6.950[-5]	1889 970	-0.2385	4.403[-3]	4579 000	0.1642	8.619[-4]
$3s4p \text{ } ^3P_1$	175 336	-0.1909	3.052[-2]	1882 746	0.1483	1.709[-3]	4541 000	0.1160	4.335[-4]
$\alpha_0(3s^2 \text{ } ^1S_0, n)$			1.151[1]			3.166[-1]			7.682[-2]
$\alpha_c$			1.624[-1]			5.616[-3]			1.203[-3]
$\alpha_{vc}$			-5.427[-3]			-9.818[-5]			-1.767[-5]
Total			1.167[1]			3.221[-1]			7.801[-2]
Mg-like Mo <sup>30+</sup>									
$3s3p \text{ } ^3P_1$	525 030	0.1346	5.048[-3]	770 400	-0.1420	3.829[-3]	1252 000	0.1171	1.603[-3]
$3s3p \text{ } ^1P_1$	862 060	0.4490	3.422[-2]	1590 900	0.3195	9.389[-3]	4403 000	-0.2122	1.496[-3]
$3s4p \text{ } ^1P_1$	6782 000	0.1363	4.009[-4]	12 630 000	-0.0955	1.056[-4]	27 160 000	-0.0152	1.236[-6]
$3s4p \text{ } ^3P_1$	6698 800	-0.1005	2.205[-4]	12 370 000	0.0787	7.323[-5]	26 430 000	0.0566	1.773[-5]
$\alpha_0(3s^2 \text{ } ^1S_0, n)$			3.991[-2]			1.341[-2]			3.136[-3]
$\alpha_c$			5.920[-4]			1.885[-4]			4.453[-5]
$\alpha_{vc}$			-8.409[-6]			-2.759[-6]			-8.371[-7]
Total			4.049[-2]			1.360[-2]			3.180[-3]
Mg-like Fe <sup>14+</sup>									
Mg-like Kr <sup>24+</sup>									
Mg-like Xe <sup>42+</sup>									
Mg-like W <sup>62+</sup>									

where the sum over  $ll' \text{ } ^{1,3}L_N$  is a sum over all states included in the odd-parity *complex* with  $J = 1$  and  $J = 3$  in the case of the dipole ( $N = 1$ ) and octupole ( $N = 3$ ) polarizabilities. In the case of quadrupole ( $N = 2$ ) polarizability, the sum over  $ll' \text{ } ^{1,3}L_1$  is a sum over all states included in the even-parity *complex* with  $J = 2$ .

### A. Dipole ground-state static polarizabilities in Mg-like ions

In the case of the dipole polarizability,  $N = 1$  and the  $3l'nl^{1,3}L_1$  *complex* consists of the five  $3l'3l^{1,3}L_1$  states ( $3s3p \text{ } ^{1,3}P_1$  and  $3p3d \text{ } ^{1,3}P_1, \text{ } ^3D_1$ ) and the thirteen  $3l'4l \text{ } ^{1,3}L_1$  states ( $3s4p \text{ } ^{1,3}P_1, \text{ } ^3P_1, \text{ } ^3P_2, \text{ } ^3P_3, \text{ } ^3D_1, \text{ } ^3D_2, \text{ } ^3D_3, \text{ } ^3F_1, \text{ } ^3F_2, \text{ } ^3F_3, \text{ } ^3G_1, \text{ } ^3G_2, \text{ } ^3G_3$ ). In Table IV, we list the contributions to dipole polarizability of the  $3s^2 \text{ } ^1S_0$  ground state in Mg-like ions with  $Z = 14, 26, 36, 42, 54$ , and  $74$ . The following designations are used in the table [52]:

$$\alpha_0(3s^2 \text{ } ^1S_0, n) = \sum_{l,l'} I(3l'nl^{(1,3)}L_1),$$

$$I(3l'nl^{(1,3)}L_1) = \frac{2}{3} \frac{|\langle 3s^2 \text{ } ^1S_0 | D | 3l'nl^{(1,3)}L_1 \rangle|^2}{E(3s^2 \text{ } ^1S_0) - E(3l'nl^{(1,3)}L_1)}. \quad (16)$$

We also use the short labels  $E(3s^2 \text{ } ^1S_0) - E(3l'nl^{(1,3)}L_1) = \Delta E$  and  $\langle 3s^2 \text{ } ^1S_0 | D | 3l'nl^{(1,3)}L_1 \rangle = D$ . In Table IV, we list the four dominant contributions among the 18 contributions including the  $3s^2 \text{ } ^1S_0-3l'nl^{(1,3)}L_1$  transitions with  $n = 3$  and  $4$ . The sum of these 18 contributions to  $\alpha_0(3s^2 \text{ } ^1S_0)$  is given in the fifth row of data [ $\alpha_0(3s^2 \text{ } ^1S_0, n)$ ] in Table IV. The contributions from the core and  $vc$  terms are given in rows “ $\alpha_c$ ” and “ $\alpha_{vc}$ .” The scalar polarizability  $\alpha_0$  is separated into a valence polarizability  $\alpha_0^v$ , an ionic core polarizability  $\alpha_c$ , and

a small term  $vc$  that modifies the ionic core polarizability due to the presence of two valence electrons [56]. The latter two terms are evaluated in the RPA [57]. The final polarizability values are listed in the “total” rows in Table IV.

The largest contribution to the polarizability of the  $3s^2 \text{ } ^1S_0$  ground state in Mg-like ions with  $Z = 14-42$  comes from the  $3s^2 \text{ } ^1S_0-3s3p \text{ } ^1P_1$  transition since the value of  $I(3s3p \text{ } ^1P_1)$  is almost equal to the  $\alpha_0(3s^2 \text{ } ^1S_0, n)$  value. All other  $3s^2 \text{ } ^1S_0-3lnl^{1,3}L_1$  transitions contribute 1% for Si<sup>2+</sup>, 3% for Fe<sup>14+</sup>, 8% for Kr<sup>24+</sup>, and 14% for Mo<sup>30+</sup>. These increasing contributions of the other terms are due to the influence of relativistic effects. The ratio of the  $I(3s3p \text{ } ^3P_1)$  and  $I(3s3p \text{ } ^1P_1)$  terms is equal to 0.4 for Mg-like Xe<sup>42+</sup> and becomes 1.1 for Mg-like W<sup>62+</sup>.

The contribution of the relativistic effects is illustrated in Fig. 4, where we plot the contributions to the electric-dipole polarizabilities of the  $3s^2 \text{ } ^1S_0$  ground state as a function of  $Z$ . We illustrate the contributions of five channels:  $3s^2 \text{ } ^1S_0-3s3p \text{ } ^1P_1$ ,  $3s^2 \text{ } ^1S_0-3s3p \text{ } ^3P_1$ ,  $3s^2 \text{ } ^1S_0-3p3d \text{ } ^1P_1$ ,  $3s^2 \text{ } ^1S_0-3s4p \text{ } ^1P_1$ , and  $3s^2 \text{ } ^1S_0-3s4p \text{ } ^3P_1$ . The dominant  $3s^2 \text{ } ^1S_0-3s3p \text{ } ^1P_1$  contribution decreases with increasing  $Z$ , while the  $3s^2 \text{ } ^1S_0-3s3p \text{ } ^3P_1$  contribution increases with  $Z$  and becomes larger than the first one around  $Z = 73$ . The value of  $\alpha_0(3s^2 \text{ } ^1S_0-3s4p \text{ } ^1P_1)$ , described by curve 4 is larger than the  $\alpha_0(3s^2 \text{ } ^1S_0-3s3p \text{ } ^3P_1)$  value (curve 2) for ions with  $Z = 13-28$ . In Fig. 4, we display the contributions from two transitions,  $3s^2 \text{ } ^1S_0-3p3d \text{ } ^1P_1$  and  $3s^2 \text{ } ^1S_0-3s4p \text{ } ^3P_1$ . The value of  $\alpha_0(3s^2 \text{ } ^1S_0-3s4p \text{ } ^3P_1)$ , described by curve 5, is larger than the value of  $\alpha_0(3s^2 \text{ } ^1S_0-3s4p \text{ } ^1P_1)$  (curve 4) for high- $Z$  ions, with  $Z > 61$ . The values of  $\alpha_0(3s^2 \text{ } ^1S_0-3p3d \text{ } ^1P_1)$ , described by curve 3, are smaller than the four other contributions for the entire interval of  $Z$ . This is why we did not include the

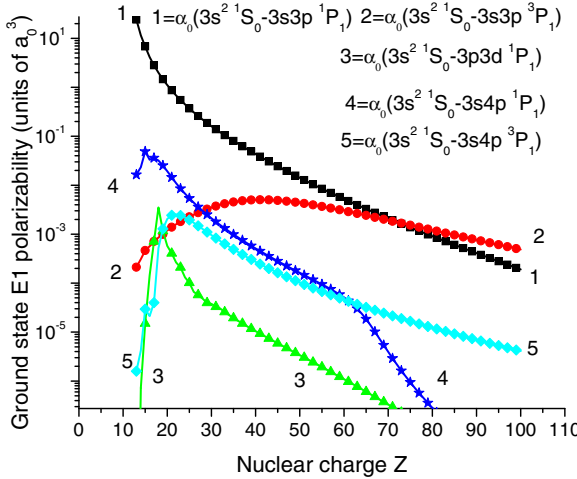


FIG. 4. (Color online) Ground-state dipole polarizability in Mg-like ions as a function of  $Z$ . The values of polarizability presented here are in units of  $a_0^3$ , where  $a_0 = 0.052\,918\text{ nm}$  is the Bohr radius.

$3s^2\ ^1S_0-3p3d\ ^1P_1$  transition in the list of dominant transitions in Table IV.

The data for the ground-state dipole polarizability  $\alpha_0(3s^2\ ^1S_0)$  are listed for Mg-like ions with  $Z = 13-100$  in Table V. The RMBPT-1 and RMBPT  $\alpha_0(3s^2\ ^1S_0)$  values are compared with the semiempirical results obtained by Reshetnikov *et al.* [34]. In that paper, the polarizabilities were calculated using the lifetime measurements for the lowest resonance transition. The difference between our RMBPT values and the results from [34] is about 1%-5% in most cases,

except the results for Mg-like  $\text{Fe}^{12+}$  (7%) and Mg-like  $\text{Ni}^{14+}$  (16%). To estimate the accuracy of our results for these ions, we additionally calculated the oscillator strength  $f$  for the  $3s^2\ ^1S_0-3s3p\ ^1P_1$  transition, along with the  $3s3p\ ^1P_1$  lifetime. These data were given in Ref. [34], as well as by Safronova *et al.* [33] and Tachiev and Froese Fischer [58]. Our values of the oscillator strength and lifetime are in excellent agreement with results from Refs. [33] and [58], while they disagree with the results from Ref. [34]. We already mentioned that the  $3s^2\ ^1S_0-3s3p\ ^1P_1$  transition gives the dominant contribution in the  $\alpha_0(3s^2\ ^1S_0)$  dipole polarizability. An additional assessment of the accuracy of our RMBPT  $\alpha_0(3s^2\ ^1S_0)$  values is given by the first-order RMBPT-1 values listed in Table V. The difference between the RMBPT-1 and the RMBPT  $\alpha_0(3s^2\ ^1S_0)$  values is about 1% for almost all Mg-like ions, except the three ions with the smallest degree of ionization:  $\text{Al}^+$ ,  $\text{Si}^{2+}$ , and  $\text{P}^{3+}$ . That means that the first-order perturbation theory method does not produce accurate results. Fortunately, the second-order RMBPT leads to much better agreement with the results obtained with the other methods.

## B. Quadrupole ground-state static polarizabilities in Mg-like ions

In the case of quadrupole polarizability,  $N = 2$  and the  $3l'nl\ ^1,3L_2$  complex consists of the seven  $3l'3l\ ^1,3L_2$  states ( $3s3d\ ^1,3D_2$ ,  $3p^2\ ^3P_2$ ,  $1D_2$  and  $3d^2\ ^3P_2$ ,  $1D_2$ ,  $3^3F_2$ ) and the fourteen  $3l'4l\ ^1,3L_2$  states ( $3s4d\ ^1,3D_2$ ,  $3p4p\ ^3P_2$ ,  $1^1D_2$ ,  $4s3d\ ^1,3D_2$ ,  $3d4d\ ^3P_2$ ,  $1^3D_2$ ,  $3^3F_2$ , and  $3p4f\ ^1,3D_2$ ,  $3^3F_2$ ). In Table VI, we list the contributions to the quadrupole polarizability of the  $3s^2\ ^1S_0$  ground state in Mg-like ions with  $Z = 14, 26, 36, 42, 54$ , and 74. The designations used in this table are

TABLE V. Electric-dipole polarizability (in  $a_0^3$ ) for Mg-like ions evaluated in the first-order RMBPT-I (a) and the second-order RMBPT (b). Our results are compared with semiempirical results obtained by Reshetnikov *et al.* [34]. A[B] means  $A \times 10^B$ .

Semiempirical												
$Z$	a	b	[34]	$Z$	a	b	$Z$	a	b	$Z$	a	b
13	2.037[1]	2.286[1]	24.20	35	8.908[-2]	8.792[-2]	57	1.077[-2]	1.068[-2]	79	2.326[-3]	2.315[-3]
14	1.037[1]	1.167[1]	11.666	36	7.903[-2]	7.801[-2]	58	9.957[-3]	9.874[-3]	80	2.187[-3]	2.176[-3]
15	6.124[0]	6.415[0]	6.312	37	7.032[-2]	6.942[-2]	59	9.215[-3]	9.140[-3]	81	2.057[-3]	2.047[-3]
16	4.347[0]	4.271[0]	4.49	38	6.277[-2]	6.198[-2]	60	8.892[-3]	8.821[-3]	82	1.935[-3]	1.926[-3]
17	2.941[0]	2.908[0]	2.77	39	5.620[-2]	5.551[-2]	61	7.916[-3]	7.855[-3]	83	1.821[-3]	1.813[-3]
18	2.089[0]	2.062[0]	2.00	40	5.046[-2]	4.984[-2]	62	7.347[-3]	7.291[-3]	84	1.715[-3]	1.708[-3]
19	1.540[0]	1.518[0]	1.48	41	4.539[-2]	4.484[-2]	63	6.825[-3]	6.775[-3]	85	1.617[-3]	1.610[-3]
20	1.106[0]	1.105[0]	1.06	42	4.097[-2]	4.049[-2]	64	6.346[-3]	6.300[-3]	86	1.524[-3]	1.518[-3]
21	9.081[-1]	9.035[-1]	0.914	43	3.702[-2]	3.659[-2]	65	5.906[-3]	5.864[-3]	87	1.437[-3]	1.431[-3]
22	7.195[-1]	7.124[-1]	0.730	44	3.354[-2]	3.316[-2]	66	5.500[-3]	5.462[-3]	88	1.356[-3]	1.351[-3]
23	5.795[-1]	5.734[-1]	0.591	45	3.046[-2]	3.012[-2]	67	5.126[-3]	5.092[-3]	89	1.279[-3]	1.275[-3]
24	4.733[-1]	4.673[-1]	0.488	46	2.770[-2]	2.740[-2]	68	4.782[-3]	4.751[-3]	90	1.208[-3]	1.204[-3]
25	3.913[-1]	3.860[-1]	0.401	47	2.524[-2]	2.497[-2]	69	4.464[-3]	4.435[-3]	91	1.141[-3]	1.136[-3]
26	3.269[-1]	3.221[-1]	0.346	48	2.303[-2]	2.279[-2]	70	4.171[-3]	4.144[-3]	92	1.079[-3]	1.075[-3]
27	2.757[-1]	2.715[-1]	0.285	49	2.105[-2]	2.084[-2]	71	3.898[-3]	3.874[-3]	93	1.020[-3]	1.017[-3]
28	2.344[-1]	2.308[-1]	0.276	50	1.927[-2]	1.908[-2]	72	3.647[-3]	3.625[-3]	94	9.645[-4]	9.617[-4]
29	2.008[-1]	1.975[-1]		51	1.767[-2]	1.749[-2]	73	3.414[-3]	3.394[-3]	95	9.124[-4]	9.119[-4]
30	1.731[-1]	1.706[-1]		52	1.622[-2]	1.606[-2]	74	3.198[-3]	3.180[-3]	96	8.637[-4]	8.606[-4]
31	1.501[-1]	1.480[-1]		53	1.490[-2]	1.477[-2]	75	2.997[-3]	2.980[-3]	97	8.176[-4]	8.142[-4]
32	1.309[-1]	1.292[-1]		54	1.372[-2]	1.360[-2]	76	2.811[-3]	2.796[-3]	98	7.745[-4]	7.719[-4]
33	1.146[-1]	1.131[-1]		55	1.264[-2]	1.253[-2]	77	2.637[-3]	2.623[-3]	99	7.340[-4]	7.314[-4]
34	1.009[-1]	9.954[-2]		56	1.166[-2]	1.156[-2]	78	2.476[-3]	2.464[-3]	100	6.959[-4]	6.939[-4]

TABLE VI. Contributions to the electric-quadrupole polarizability of Mg-like ions in the  $3s^2\ 1S_0$  ground state. Designations:  $\Delta E = E(3s^2\ 1S_0) - E(3l'n l^{(1,3)}L_2)$ ,  $D = \langle 3s^2\ 1S_0 \| D \| 3l'n l^{(1,3)}L_2 \rangle$ ,  $I = I(3l'n l^{(1,3)}L_2) = \frac{2}{5} \frac{| \langle 3s^2\ 1S_0 \| D \| 3l'n l^{(1,3)}L_2 \rangle |^2}{E(3s^2\ 1S_0) - E(3l'n l^{(1,3)}L_2)}$ ,  $\alpha_0(3s^2\ 1S_0, n) = \sum_{l=1,3} I(3l'n l^{(1,3)}L_2)$ . All values are in a.u. Excitation energies (in cm<sup>-1</sup>) and absolute values of the corresponding reduced electric-dipole matrix elements are listed in columns “ $\Delta E$ ” and “ $D$ .”  $I$  values are calculated with NIST energies [48] or with RMBPT energies when NIST energies are absent. Contributions from the core and  $v_c$  terms are listed in rows “ $\alpha_c$ ” and “ $\alpha_{vc}$ .” Final polarizability values are listed in “total” rows.  $A[B]$  means  $A \times 10^B$ .

Level	$\Delta E$ (cm <sup>-1</sup> )	$D$ (a.u.)	$I(a_0^3)$	$\Delta E$ (cm <sup>-1</sup> )	$D$ (a.u.)	$I(a_0^3)$	$\Delta E$ (cm <sup>-1</sup> )	$D$ (a.u.)	$I(a_0^3)$
Mg-like Si <sup>2+</sup>									
$3p2\ ^1D_2$	122 215	5.2398	1.972[1]	559 600	0.399 22	2.499[-2]	996 610	0.1438	1.822[-3]
$3p2\ ^3P_2$	130 101	0.0855	4.938[-3]	581 803	0.175 03	4.621[-3]	1092 830	0.1023	8.413[-4]
$3s3d\ ^3D_2$	142 946	0.0015	1.443[-6]	679 785	0.003 76	1.754[-6]	1184 970	0.0051	1.919[-6]
$3s3d\ ^1D_2$	165 765	4.9295	1.287[1]	762 093	0.469 02	2.534[-2]	1319 434	0.1855	2.290[-3]
$3s4d\ ^3D_2$	201 598	0.0003	4.977[-8]	2032 020	0.066 84	1.927[-4]	4816 832	0.0834	1.268[-4]
$3s4d\ ^1D_2$	204 331	0.2619	2.973[-2]	2035 280	0.522 12	1.176[-2]	4827 388	0.2390	1.039[-3]
$\alpha_0(3s^2\ 1S_0, n)$			3.328[1]			6.756[-2]			6.148[-3]
$\alpha_c$			9.562[-2]			5.896[-4]			5.766[-5]
Total			3.328[1]			6.815[-2]			6.206[-3]
Mg-like Mo <sup>30+</sup>									
$3p2\ ^1D_2$	1329 950	0.0927	5.674[-4]	2284 367	0.0462	8.198[-5]	5535 299	0.0199	6.310[-6]
$3p2\ ^3P_2$	1518 870	0.0851	4.185[-4]	2582 629	0.0242	1.997[-5]	5930 433	0.0156	3.617[-6]
$3s3d\ ^3D_2$	1560 630	0.0100	5.626[-6]	2769 805	0.0725	1.667[-4]	6638 292	0.0356	1.677[-5]
$3s3d\ ^1D_2$	1739 970	0.1184	7.073[-4]	3060 202	0.0315	2.855[-5]	8587 871	0.0019	3.571[-8]
$3s4d\ ^3D_2$	7077 640	0.0756	7.098[-5]	13 064 820	0.0530	1.884[-5]	28 291 158	0.0271	2.272[-6]
$3s4d\ ^1D_2$	7097 832	0.1604	3.183[-4]	13 128 665	0.0824	4.538[-5]	28 569 671	0.0347	3.700[-6]
$\alpha_0(3s^2\ 1S_0, n)$			2.096[-3]			3.624[-4]			3.282[-5]
$\alpha_c$			1.980[-5]			3.493[-6]			3.851[-7]
Total			2.116[-3]			3.659[-4]			3.321[-5]
Mg-like Fe <sup>14+</sup>									
Mg-like Kr <sup>24+</sup>									
Mg-like Xe <sup>42+</sup>									
Mg-like W <sup>62+</sup>									

similar to Eq. (16):

$$\alpha_0(3s^2\ 1S_0, n) = \sum_{l=1,3} I(3l'n l^{(1,3)}L_2), \quad (17)$$

$$I(3l'n l^{(1,3)}L_2) = \frac{2}{5} \frac{| \langle 3s^2\ 1S_0 \| D \| 3l'n l^{(1,3)}L_2 \rangle |^2}{E(3s^2\ 1S_0) - E(3l'n l^{(1,3)}L_2)}.$$

We also use the short labels  $E(3s^2\ 1S_0) - E(3l'n l^{(1,3)}L_2) = \Delta E$  and  $\langle 3s^2\ 1S_0 \| D \| 3l'n l^{(1,3)}L_2 \rangle = D$ . In Table VI, we list the six dominant contributions among the 18 contributions including the  $3s^2\ 1S_0 - 3l'n l^{(1,3)}L_2$  transitions with  $n = 3$  and 4. The sum of these 21 contributions to  $\alpha_0(3s^2\ 1S_0)$  are given in the seventh row of data [ $\alpha_0(3s^2\ 1S_0, n)$ ] in Table VI. The contribution from the core is given in rows “ $\alpha_c$ .” This term is evaluated in the RPA [57]. The final polarizability values are listed in the “total” rows in Table VI.

It should be noted that the  $\langle 3s^2\ 1S_0 \| D \| 3l'n l^{(1,3)}L_2 \rangle = D$  values in Table VI are evaluated in the length form. To check the accuracy of our results, we evaluated these matrix elements in the velocity form. A comparison of  $E2$  polarizabilities calculated in the length and velocity form shows excellent agreement. The  $L - V$  difference in  $\alpha_0(3s^2\ 1S_0)$  is about 1%–5% for the RMBPT-1 values and 0.5%–1.5% for the RMBPT values for Mg-like ions with  $Z = 14$ –100.

The largest contributions to the quadrupole polarizability of the  $3s^2\ 1S_0$  ground state in Mg-like ions with  $Z = 14$ –46 comes from the  $3s^2\ 1S_0 - 3p^2\ ^1D_2$  and  $3s^2\ 1S_0 - 3s3d\ ^1D_2$  transitions. Only a 2% contribution comes from other terms for Si<sup>2+</sup>. The third important contribution for the  $E2$  polarizability comes

from the  $3s^2\ 1S_0 - 3s4d\ ^1D_2$  transition. This term contributes 17% to the  $E2$  polarizability in Mg-like Fe<sup>14+</sup> and Kr<sup>24+</sup>. It contributes somewhat less to Mo<sup>30+</sup> (15%), Xe<sup>42+</sup> (13%), and W<sup>62+</sup> (11%). The largest contribution (51%) to the  $E2$  polarizability of Mg-like W<sup>62+</sup> comes from the  $3s^2\ 1S_0 - 3s3d\ ^3D_2$  intercombination transition.

The contribution of the relativistic effects is illustrated in Fig. 5, where we plot the contributions to the electric-quadrupole polarizabilities of the  $3s^2\ 1S_0$  ground state in

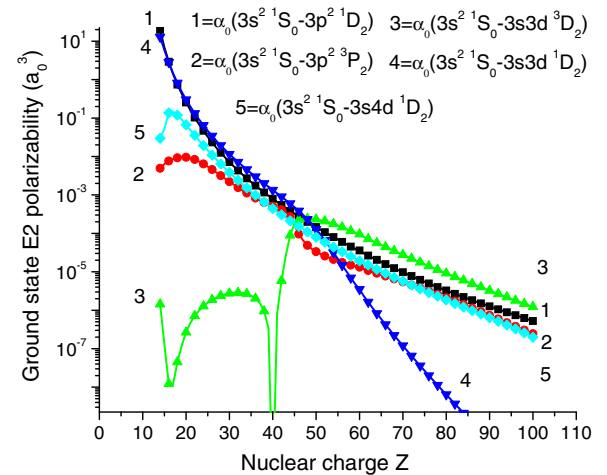


FIG. 5. (Color online) Ground-state quadrupole polarizability in Mg-like ions as a function of  $Z$ . The values of polarizability presented here are in units of  $a_0^3$ , where  $a_0 = 0.052\ 918$  nm is the Bohr radius.

TABLE VII. Electric-quadrupole polarizability (in  $a_0^3$ ) for Mg-like ions evaluated in the first-order RMBPT-I (a) and the second-order RMBPT (b).  $A[B]$  means  $A \times 10^B$ .

Z	a	b	Z	a	b	Z	a	b	Z	a	b
13	9.369[1]	1.121[2]	35	7.503[-3]	7.575[-3]	57	2.383[-4]	2.447[-4]	79	1.938[-5]	1.958[-5]
14	2.810[1]	3.338[1]	36	6.149[-3]	6.206[-3]	58	2.099[-4]	2.148[-4]	80	1.747[-5]	1.766[-5]
15	1.105[1]	1.298[1]	37	5.069[-3]	5.117[-3]	59	1.852[-4]	1.890[-4]	81	1.576[-5]	1.593[-5]
16	5.131[0]	5.953[0]	38	4.201[-3]	4.243[-3]	60	1.696[-4]	1.727[-4]	82	1.422[-5]	1.438[-5]
17	2.667[0]	3.066[0]	39	3.501[-3]	3.539[-3]	61	1.448[-4]	1.472[-4]	83	1.285[-5]	1.299[-5]
18	1.502[0]	1.716[0]	40	2.933[-3]	2.968[-3]	62	1.283[-4]	1.302[-4]	84	1.161[-5]	1.174[-5]
19	9.002[-1]	1.021[0]	41	2.466[-3]	2.499[-3]	63	1.139[-4]	1.154[-4]	85	1.050[-5]	1.062[-5]
20	5.654[-1]	6.436[-1]	42	2.084[-3]	2.116[-3]	64	1.012[-4]	1.024[-4]	86	9.496[-6]	9.610[-6]
21	3.701[-1]	3.999[-1]	43	1.767[-3]	1.795[-3]	65	8.996[-5]	9.101[-5]	87	8.594[-6]	8.699[-6]
22	2.501[-1]	2.638[-1]	44	1.503[-3]	1.527[-3]	66	8.011[-5]	8.099[-5]	88	7.782[-6]	7.879[-6]
23	1.736[-1]	1.814[-1]	45	1.284[-3]	1.309[-3]	67	7.143[-5]	7.218[-5]	89	7.049[-6]	7.139[-6]
24	1.234[-1]	1.281[-1]	46	1.100[-3]	1.129[-3]	68	6.375[-5]	6.440[-5]	90	6.388[-6]	6.471[-6]
25	8.955[-2]	9.243[-2]	47	9.458[-4]	9.770[-4]	69	5.695[-5]	5.752[-5]	91	5.791[-6]	5.867[-6]
26	6.616[-2]	6.815[-2]	48	8.153[-4]	8.467[-4]	70	5.094[-5]	5.144[-5]	92	5.252[-6]	5.323[-6]
27	4.965[-2]	5.103[-2]	49	7.047[-4]	7.347[-4]	71	4.560[-5]	4.604[-5]	93	4.765[-6]	4.830[-6]
28	3.780[-2]	3.860[-2]	50	6.106[-4]	6.383[-4]	72	4.086[-5]	4.125[-5]	94	4.324[-6]	4.384[-6]
29	2.913[-2]	2.966[-2]	51	5.305[-4]	5.548[-4]	73	3.663[-5]	3.699[-5]	95	3.925[-6]	3.980[-6]
30	2.271[-2]	2.307[-2]	52	4.619[-4]	4.825[-4]	74	3.289[-5]	3.321[-5]	96	3.563[-6]	3.614[-6]
31	1.789[-2]	1.814[-2]	53	4.030[-4]	4.199[-4]	75	2.954[-5]	2.983[-5]	97	3.236[-6]	3.283[-6]
32	1.422[-2]	1.440[-2]	54	3.525[-4]	3.659[-4]	76	2.656[-5]	2.682[-5]	98	2.940[-6]	2.983[-6]
33	1.141[-2]	1.154[-2]	55	3.088[-4]	3.194[-4]	77	2.389[-5]	2.413[-5]	99	2.672[-6]	2.711[-6]
34	9.218[-3]	9.312[-3]	56	2.710[-4]	2.792[-4]	78	2.150[-5]	2.173[-5]	100	2.427[-6]	2.466[-6]

Mg-like ions as a function of  $Z$ . We illustrate the contributions of five channels: the  $3s^2\ 1S_0-3p^2\ 1D_2$ ,  $3s^2\ 1S_0-3p^2\ 3P_2$ ,  $3s^2\ 1S_0-3s3d\ 3D_2$ ,  $3s^2\ 1S_0-3s3d\ 1D_2$ , and  $3s^2\ 1S_0-3s4d\ 1D_2$  transitions (curves 1–5, respectively). The  $3s^2\ 1S_0-3s3d\ 1D_2$  contribution (curve 4) decreases with increasing  $Z$  and becomes smaller than the other four contributions at  $Z > 59$ . The smallest  $3s^2\ 1S_0-3s3d\ 3D_2$  contribution (curve 3) at  $Z = 13$ –44 increases with  $Z$  and becomes larger than the other four contributions around  $Z = 47$ . The ratio of the values of  $\alpha_0(3s^2\ 1S_0-3p^2\ 1D_2)$  and  $\alpha_0(3s^2\ 1S_0-3p^2\ 3D_2)$ , described by curves 1 and 2 in Fig. 5, varies slowly from 2 to 5 for high- $Z$  ions.

The tabulated data for the ground-state quadrupole polarizability  $\alpha_0(3s^2\ 1S_0)$  are listed for Mg-like ions with  $Z = 13$ –100 in Table VII. The difference between the RMBPT-1 and the RMBPT  $\alpha_0(3s^2\ 1S_0)$  values is about 1%–4% for almost all Mg-like ions except for those with a small degree of ionization: Al<sup>+</sup>–Ti<sup>10+</sup>, where the difference is about 10%–15%. This means that the correlation effects for the  $E2$  polarizability decreases less slowly with  $Z$  than those found for the  $E1$  polarizability.

The ground-state quadrupole polarizability of the Si<sup>2+</sup> ion had been calculated earlier by Mitroy [36] using a large-scale CI calculation and the sum-over-states approach. The difference between our RMBPT value ( $33.38a_0^3$ ) and the result from [36] ( $35.754a_0^3$ ) is about 6.6%. Unfortunately, we did not find any other theoretical results for comparison.

### C. Octupole ground-state static polarizabilities in Mg-like ions

In the case of octupole polarizability,  $N = 3$  and the  $3l'n l^{1,3}L_3$  complex consists of the three  $3p3d\ 3D_3$ ,  $1,3F_3$  states and the twelve  $3l'4l\ 1,3L_3$  states ( $3s4f\ 1,3F_3$ ,  $3p4d\ 3D_3$ ,  $1,3F_3$ ,

$3d4p\ 3D_3$ ,  $1,3F_3$ , and  $3d4f\ 3D_3$ ,  $1,3F_3$ ,  $3G_3$ ). In Table VIII, we list the contributions to the octupole polarizability of the  $3s^2\ 1S_0$  ground state in Mg-like ions with  $Z = 14$ , 26, 36, 42, 54, and 74. The designations used in this table are similar to Eqs. (16) and (17):

$$\alpha_0(3s^2\ 1S_0, n) = \sum_{1,3Ll'} I(3l'n l^{(1,3)}L_3), \quad (18)$$

$$I(3l'n l^{(1,3)}L_2) = \frac{2}{7} \frac{\langle |3s^2\ 1S_0| D |3l'n l^{(1,3)}L_3 \rangle|^2}{(E(3s^2\ 1S_0) - E(3l'n l^{(1,3)}L_3))}.$$

We also use the short labels  $E(3s^2\ 1S_0) - E(3l'n l^{(1,3)}L_3) = \Delta E$  and  $\langle 3s^2\ 1S_0 | D | 3l'n l^{(1,3)}L_3 \rangle = D$ . In Table VIII, we list the five dominant contributions among the 15 contributions including the  $3s^2\ 1S_0-3l'n l^{(1,3)}L_3$  transitions with  $n = 3$  and 4. The sum of these 15 contributions in the  $\alpha_0(3s^2\ 1S_0)$  is given in the sixth row of data [ $\alpha_0(3s^2\ 1S_0, n)$ ] in Table VIII. The contributions from the core are given in rows “ $\alpha_c$ .” This term is evaluated in the RPA [57]. Final polarizability values are listed in “total” rows in Table VIII.

The largest contribution to the octupole polarizability of the  $3s^2\ 1S_0$  ground state in Mg-like ions with  $Z = 14$ –100 comes from the  $3s^2\ 1S_0-3s4f\ 1F_3$  transition. Only a 5%–6% contribution comes from other terms for Fe<sup>14+</sup>, Kr<sup>24+</sup>, and Mo<sup>30+</sup>. The second most important contribution to the  $E3$  polarizability of Si<sup>2+</sup> comes from the  $3s^2\ 1S_0-3p3d\ 1F_3$  transition, while for high- $Z$  ions (Mg-like Xe<sup>42+</sup> and W<sup>62+</sup>) it comes from the  $3s^2\ 1S_0-3s4f\ 3F_3$  intercombination transition.

The contribution of the relativistic effects is illustrated in Fig. 6, where we plot the contributions to the electric-octupole polarizabilities of the  $3s^2\ 1S_0$  ground state as a function of  $Z$ . We illustrate the contributions of

TABLE VIII. Contributions to the electric-octupole polarizability of Mg-like ions in the  $3s^2 1S_0$  ground state. Designations:  $\Delta E = E(3s^2 1S_0) - E(3l'n l^{(1,3)}L_3)$ ,  $D = \langle 3s^2 1S_0 | D | 3l'n l^{(1,3)}L_3 \rangle$ ,  $I = I(3l'n l^{(1,3)}L_3) = \frac{2}{7} \frac{| \langle 3s^2 1S_0 | D | 3l'n l^{(1,3)}L_3 \rangle |^2}{E(3s^2 1S_0) - E(3l'n l^{(1,3)}L_3)}$ ,  $\alpha_0(3s^2 1S_0, n) = \sum_{l=1,3} I(3l'n l^{(1,3)}L_3)$ . All values are in a.u. Excitation energies (in  $\text{cm}^{-1}$ ) and absolute values of the corresponding reduced electric-dipole matrix elements are listed in columns “ $\Delta E$ ” and “ $D$ .”  $I$  values are calculated with NIST energies [48] or with RMBPT energies when NIST energies are absent. Contributions from the core and  $v_c$  terms are listed in rows “ $\alpha_c$ ” and “ $\alpha_{vc}$ .” Final polarizability values are listed in “total” rows.  $A[B]$  means  $A \times 10^B$ .

Level	$\Delta E$ (cm $^{-1}$ )	$D$ (a.u.)	$I(a_0^3)$	$\Delta E$ (cm $^{-1}$ )	$D$ (a.u.)	$I(a_0^3)$	$\Delta E$ (cm $^{-1}$ )	$D$ (a.u.)	$I(a_0^3)$
Mg-like Si $^{2+}$									
$3p3d\ ^3F_3$	199 026	0.0470	6.961[-4]	938 126	0.0116	9.008[-6]	1645 700	0.0078	2.296[-6]
$3p3d\ ^3D_3$	217 489	0.0429	5.299[-4]	994 852	0.0120	9.006[-6]	1765 500	0.0073	1.910[-6]
$3p3d\ ^1F_3$	235 414	9.0130	2.164[1]	1062 515	0.1582	1.477[-3]	1869 500	0.0326	3.572[-5]
$3s4f\ ^3F_3$	204 828	0.0088	2.350[-5]	2108 420	0.0095	2.685[-6]	4964 073	0.0121	1.835[-6]
$3s4f\ ^1F_3$	209 559	22.4386	1.507[2]	2123 150	0.8975	2.379[-2]	4990 008	0.2479	7.721[-4]
$\alpha_0(3s^2 1S_0, n)$			1.738[2]			2.537[-2]			8.158[-4]
$\alpha_c$			1.041[-1]			9.897[-5]			4.242[-6]
Total			1.739[2]			2.547[-2]			8.200[-4]
Mg-like Mo $^{30+}$									
$3p3d\ ^3F_3$	2162 220	0.0060	1.044[-6]	3550 057	0.0031	1.731[-7]	7888 737	0.0010	7.351[-9]
$3p3d\ ^3D_3$	2362 430	0.0055	7.918[-7]	4104 079	0.0027	1.138[-7]	10 205 527	0.0007	2.936[-9]
$3p3d\ ^1F_3$	2490 670	0.0157	6.209[-6]	4330 521	0.0043	2.724[-7]	10 948 353	0.0007	3.005[-9]
$3s4f\ ^3F_3$	7275 100	0.0127	1.398[-6]	13 376 029	0.0123	7.039[-7]	28 921 811	0.0077	1.287[-7]
$3s4f\ ^1F_3$	7335 700	0.1385	1.639[-4]	13 432 501	0.0538	1.353[-5]	29 072 530	0.0154	5.129[-7]
$\alpha_0(3s^2 1S_0, n)$			1.738[-4]			1.482[-5]			6.556[-7]
$\alpha_c$			1.002[-6]			9.825[-8]			5.271[-9]
Total			1.748[-4]			1.492[-5]			6.609[-7]
Mg-like Fe $^{14+}$									
Mg-like Kr $^{24+}$									
Mg-like Xe $^{42+}$									
Mg-like W $^{62+}$									

five channels:  $3s^2 1S_0 - 3p3d\ ^3F_3$ ,  $3s^2 1S_0 - 3p3d\ ^3D_3$ ,  $3s^2 1S_0 - 3p3d\ ^1F_3$ ,  $3s^2 1S_0 - 3s4f\ ^3F_3$ , and  $3s^2 1S_0 - 3s4f\ ^1F_3$ . The value of  $\alpha_0(3s^2 1S_0 - 3s4f\ ^3F_3)$ , described by curve 5, dominates for all values of  $Z$ . The value of  $\alpha_0(3s^2 1S_0 - 3p3d\ ^1F_3)$ , described by curve 3, is larger than the values described by curves 1, 2, and 4 for ions with  $Z = 14-49$  and becomes the smallest contribution for high- $Z$  ions. The value of  $\alpha_0(3s^2 1S_0 - 3s4f\ ^3F_3)$ , described by curve 4, is smaller than the values described by curves 1, 2, and 3 for ions with  $Z = 14-49$  and becomes larger than the values described by curves 1, 2, and 3 for high- $Z$  ions.

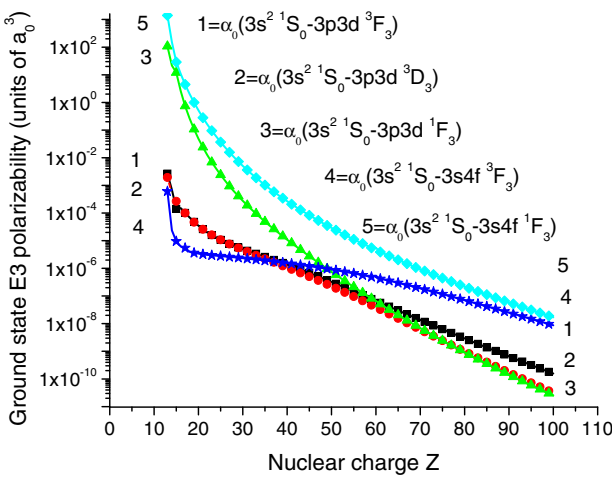


FIG. 6. (Color online) Ground-state octupole polarizability in Mg-like ions as a function of  $Z$ . The values of polarizability presented here are in units of  $a_0^3$ , where  $a_0 = 0.052 918 \text{ nm}$  is the Bohr radius.

The tabulated data for the ground-state octupole polarizability  $\alpha_0(3s^2 1S_0)$  are listed for Mg-like ions with  $Z = 14-100$  in Table IX. The difference between the RMBPT-1 and the RMBPT  $\alpha_0(3s^2 1S_0)$  values is about 3%–10% for high- $Z$  ions and about 10%–20% for ions with  $Z = 16-35$ . The largest difference is found for Si $^{2+}$ , P $^{3+}$ , and S $^{4+}$ . This large difference between RMBPT-1 and RMBPT values of the  $E3$  polarizability is due to the second-order contribution. The values arising from the  $3s^2 1S_0 - 3p3d\ ^3F_3$ ,  $3s^2 1S_0 - 3p3d\ ^3D_3$ , and  $3s^2 1S_0 - 3p3d\ ^1F_3$  transitions are not 0 due to the second-order contribution [see  $T_3^{(\text{corr})}$  in Eq. (8)] and mixing of the configurations. From another side, we can see in Table I that the difference in the  $E3$  reduced matrix elements  $Q$  calculated in length  $L$  versus velocity  $V$  forms for Fe $^{14+}$  is less than 2%.

The ground-state octupole polarizability of the Si $^{2+}$  ion was calculated by Mitroy [36] based on a large-scale CI calculation using the sum-over-states approach. The difference between our RMBPT value ( $173.9 a_0^3$ ) and the result from [36] ( $171.85 a_0^3$ ) is about 2.2%. Unfortunately, we did not find any other theoretical  $E3$  polarizability results for comparison.

## V. UNCERTAINTY ESTIMATES AND CONCLUSION

We have presented a systematic second-order relativistic MBPT study of the multipole contributions to the lifetime of the  $3s3p\ ^3P_2$  level and to the multipole ground-state static polarizabilities in Mg-like ions. The comparison of the first-order RMBPT-I and second-order RMBPT line strengths, transition rates, lifetimes, and multipole polarizabilities presented in Tables I–IX gives us an estimation of the uncertainties of our results. The comparison of the  $E1$ ,  $E2$ , and  $E3$  reduced

TABLE IX. Electric-octupole polarizability (in  $a_0^3$ ) for Mg-like ions evaluated in the first-order RMBPT-I (a) and the second-order RMBPT (b).  $A[B]$  means  $A \times 10^B$ .

Z	a	b	Z	a	b	Z	a	b	Z	a	b
14	9.731[1]	1.739[2]	35	9.820[-4]	1.092[-3]	57	8.181[-6]	8.791[-6]	79	3.230[-7]	3.389[-7]
15	2.889[1]	4.117[1]	36	7.391[-4]	8.200[-4]	58	6.909[-6]	7.415[-6]	80	2.839[-7]	2.976[-7]
16	1.015[1]	1.330[1]	37	5.615[-4]	6.217[-4]	59	5.850[-6]	6.270[-6]	81	2.497[-7]	2.616[-7]
17	4.160[0]	5.231[0]	38	4.302[-4]	4.755[-4]	60	5.890[-6]	6.285[-6]	82	2.200[-7]	2.302[-7]
18	1.879[0]	2.309[0]	39	3.322[-4]	3.666[-4]	61	4.229[-6]	4.521[-6]	83	1.939[-7]	2.028[-7]
19	9.183[-1]	1.110[0]	40	2.585[-4]	2.848[-4]	62	3.607[-6]	3.852[-6]	84	1.711[-7]	1.788[-7]
20	4.774[-1]	5.693[-1]	41	2.026[-4]	2.228[-4]	63	3.086[-6]	3.291[-6]	85	1.511[-7]	1.578[-7]
21	2.614[-1]	3.067[-1]	42	1.592[-4]	1.748[-4]	64	2.644[-6]	2.816[-6]	86	1.336[-7]	1.394[-7]
22	1.495[-1]	1.745[-1]	43	1.268[-4]	1.390[-4]	65	2.272[-6]	2.417[-6]	87	1.181[-7]	1.232[-7]
23	8.883[-2]	1.030[-1]	44	1.013[-4]	1.109[-4]	66	1.955[-6]	2.077[-6]	88	1.045[-7]	1.090[-7]
24	5.452[-2]	6.290[-2]	45	8.130[-5]	8.886[-5]	67	1.686[-6]	1.789[-6]	89	9.258[-8]	9.647[-8]
25	3.443[-2]	3.952[-2]	46	6.561[-5]	7.160[-5]	68	1.457[-6]	1.545[-6]	90	8.205[-8]	8.545[-8]
26	2.229[-2]	2.547[-2]	47	5.321[-5]	5.798[-5]	69	1.260[-6]	1.335[-6]	91	7.277[-8]	7.574[-8]
27	1.476[-2]	1.680[-2]	48	4.335[-5]	4.718[-5]	70	1.093[-6]	1.156[-6]	92	6.458[-8]	6.718[-8]
28	9.973[-3]	1.131[-2]	49	3.548[-5]	3.856[-5]	71	9.490[-7]	1.003[-6]	93	5.733[-8]	5.960[-8]
29	6.861[-3]	7.756[-3]	50	2.916[-5]	3.165[-5]	72	8.254[-7]	8.715[-7]	94	5.092[-8]	5.292[-8]
30	4.799[-3]	5.406[-3]	51	2.407[-5]	2.608[-5]	73	7.190[-7]	7.584[-7]	95	4.525[-8]	4.700[-8]
31	3.407[-3]	3.827[-3]	52	1.993[-5]	2.157[-5]	74	6.272[-7]	6.609[-7]	96	4.022[-8]	4.176[-8]
32	2.452[-3]	2.746[-3]	53	1.657[-5]	1.791[-5]	75	5.478[-7]	5.767[-7]	97	3.577[-8]	3.713[-8]
33	1.787[-3]	1.997[-3]	54	1.383[-5]	1.492[-5]	76	4.792[-7]	5.040[-7]	98	3.182[-8]	3.301[-8]
34	1.317[-3]	1.468[-3]	55	1.157[-5]	1.246[-5]	77	4.196[-7]	4.410[-7]	99	2.832[-8]	2.937[-8]
			56	9.714[-6]	1.045[-5]	78	3.680[-7]	3.864[-7]	100	2.521[-8]	2.613[-8]

matrix elements calculated in the length and velocity form gives us a second estimate of the accuracy of our results. The comparison with prior theoretical results and the available experimental measurements gives yet another estimate of the uncertainties. Unfortunately, the number of experimental data is very limited. Although there are somewhat more previous calculations than experimental data, these are also very limited and mostly confined to ions with low ionization.

We point out that an advantage of the RMBPT method is the decreasing errors with increasing degree of ionization. As

a result, we estimate that our results have an uncertainty of a few percent and probably less than 1% for the highest-Z Mg-like ions.

## ACKNOWLEDGMENT

Work by the Lawrence Livermore National Laboratory was performed under the auspices of the U.S. DOE under Contract No. DE-AC52-07NA27344.

- 
- [1] H. G. Berry, J. Bromander, and R. Buchta, *Phys. Scripta* **1**, 181 (1970).  
[2] H. G. Berry, J. Bromander, L. J. Curtis, and R. Buchta, *Phys. Scripta* **3**, 125 (1971).  
[3] L. J. Curtis, I. Martinson, and R. Buchta, *Phys. Scripta* **3**, 197 (1971).  
[4] S. Bashkin and I. Martinson, *J. Opt. Soc. Am.* **61**, 1686 (1971).  
[5] A. E. Livingston, D. J. G. Irwin, and E. H. Pinnington, *J. Opt. Soc. Am.* **62**, 1303 (1972).  
[6] S. Bashkin, J. Bromander, J. A. Leavitt, and I. Martinson, *Phys. Scripta* **8**, 285 (1973).  
[7] S. N. Bhardwaj, H. G. Berry, and T. Mossberg, *Phys. Scripta* **9**, 331 (1974).  
[8] L. J. Curtis and W. H. Smith, *Phys. Rev. A* **9**, 1537 (1974).  
[9] A. E. Livingston, J. A. Kernahan, D. J. G. Irwin, and E. H. Pinnington, *J. Phys. B* **9**, 389 (1976).  
[10] A. E. Livingston, Y. Baudinet-Robinet, H. P. Garnir, and P. D. Dumont, *J. Opt. Soc. Am.* **66**, 1393 (1976).  
[11] A. E. Livingston, E. H. Pinnington, D. J. G. Irwin, J. A. Kernahan, and R. L. Brooks, *J. Opt. Soc. Am.* **71**, 442 (1981).  
[12] E. Träbert, K. W. Jones, B. M. Johnson, D. C. Gregory, and T. H. Kruse, *Phys. Lett. A* **87**, 336 (1982).  
[13] Y. Baudinet-Robinet, P. D. Dumont, and H. P. Garnir, *Nucl. Instrum. Methods Phys. Res.* **202**, 33 (1982).  
[14] M.-C. Buchet-Poulizac, J.-P. Buchet, and P. Ceyzeriat, *Nucl. Instrum. Methods Phys. Res.* **202**, 13 (1982).  
[15] H. S. Kwong, B. C. Johnson, P. L. Smith, and W. H. Parkinson, *Phys. Rev. A* **27**, 3040 (1983).  
[16] N. Reistad, T. Brage, J. O. Ekberg, and L. Engström, *Phys. Scripta* **30**, 249 (1984).  
[17] N. Reistad, C. Jupén, S. Huldt, L. Engström, and I. Martinson, *Phys. Scripta* **32**, 164 (1985).  
[18] E. Träbert, N. Reistad, and R. Hutton, *Z. Phys. D* **1**, 331 (1986).  
[19] N. Reistad, L. Engström, and H. G. Berry, *Phys. Scripta* **34**, 158 (1986).

- [20] B. C. Johnson, P. L. Smith, and W. H. Parkinson, *Astrophys. J.* **308**, 1013 (1986).
- [21] E. Träbert, R. Hutton, and I. Martinson, *Z. Phys. D* **5**, 125 (1987).
- [22] R. Hutton, N. Reistad, I. Martinson, E. Träbert, P. H. Heckmann, J. H. Blanke, H. M. Hellmann, and R. Hucke, *Phys. Scripta* **35**, 300 (1987).
- [23] R. Hutton, L. Engström, and E. Träbert, *Nucl. Instrum. Methods Phys. Res. B* **31**, 294 (1988).
- [24] P. van der Westhuizen, T. C. Kotze, and P. B. Kotze, *J. Quant. Spectrosc. Radiat. Transfer* **41**, 363 (1989).
- [25] E. Träbert, J. Suleiman, S. Cheng, H. G. Berry, R. W. Dunford, E. P. Kanter, C. Kurtz, A. E. Livingston, K. W. Kukla, F. G. Serpa *et al.*, *Phys. Rev. A* **47**, 3805 (1993).
- [26] L. Engström, P. Bengtsson, C. Jupén, A. E. Livingston, and I. Martinson, *Phys. Rev. A* **51**, 179 (1995).
- [27] E. Träbert, E. H. Pinnington, J. A. Kernahan, J. Doerfert, J. Granzow, P. H. Heckmann, and R. Hutton, *J. Phys. B* **29**, 2647 (1996).
- [28] E. Träbert, M. Grieser, J. Hoffmann, C. Krantz, S. Reinhardt, R. Repnow, A. Wolf, and P. Indelicato, *New J. Phys.* **13**, 023017 (2011).
- [29] H. Kang, J. Li, C. Dong, and G. Gaigalas, *J. Phys. B* **43**, 095003 (2010).
- [30] M. Andersson, Y. Zou, R. Hutton, and T. Brage, *J. Phys. B* **43**, 095001 (2010).
- [31] K. M. Aggarwal, V. Tayal, G. P. Gupta, and F. P. Keenan, *At. Data Nucl. Data Tables* **93**, 615 (2007).
- [32] E. Landi, *At. Data Nucl. Data Tables* **97**, 587 (2011).
- [33] U. I. Safronova, W. R. Johnson, and H. G. Berry, *Phys. Rev. A* **61**, 052503 (2000).
- [34] N. Reshetnikov, L. J. Curtis, M. S. Brown, and R. E. Irving, *Phys. Scripta* **77**, 015301 (2008).
- [35] L. Hamonou and A. Hibbert, *J. Phys. B* **41**, 245004 (2008).
- [36] J. Mitroy, *Phys. Rev. A* **78**, 052515 (2008).
- [37] R. A. Komara, M. A. Gearba, C. W. Fehrenbach, and S. R. Lundeen, *J. Phys. B* **38**, S87 (2005).
- [38] K. Kondo, J. L. Terry, J. E. Rice, and E. S. Marmar, *Phys. Lett. A* **117**, 189 (1986).
- [39] B. Denne and I. Martinson, *Phys. Scripta* **41**, 669 (1990).
- [40] I. Kink, M. Tunklev, and U. Litzen, *J. Opt. Soc. Am. B* **14**, 722 (1997).
- [41] K. B. Fournier, A. Ya. Faenov, T. A. Pikuz, A. I. Magunov, I. Yu. Skobelev, F. Flora, S. Bollanti, P. Di Lazzaro, D. Murra, V. S. Belyaev *et al.*, *Phys. Rev. E* **70**, 016406 (2004).
- [42] W. R. Johnson, D. R. Plante, and J. Sapirstein, *Adv. Atom. Mol. Opt. Phys.* **35**, 255 (1995).
- [43] U. I. Safronova, A. Derevianko, M. S. Safronova, and W. R. Johnson, *J. Phys. B* **32**, 3527 (1999).
- [44] M. S. Safronova, W. R. Johnson, and U. I. Safronova, *Phys. Rev. A* **53**, 4036 (1996).
- [45] U. I. Safronova, W. R. Johnson, M. S. Safronova, and A. Derevianko, *Phys. Scripta* **59**, 286 (1999).
- [46] U. I. Safronova, W. R. Johnson, and A. Derevianko, *Phys. Scripta* **60**, 46 (1999).
- [47] M. H. Chen, K. T. Cheng, and W. R. Johnson, *Phys. Rev. A* **47**, 3692 (1993).
- [48] Yu. Ralchenko, F.-C. Jou, D. E. Kelleher, A. E. Kramida, A. Musgrove, J. Reader, W. L. Wiese, and K. Olsen, *NIST Atomic Spectra Database (Version 3.0.2)* (National Institute of Standards and Technology, Gaithersburg, MD, 2005). Available at: <http://physics.nist.gov/asd3>
- [49] U. I. Safronova, *Mol. Phys.* **98**, 1213 (2000).
- [50] U. I. Safronova, W. R. Johnson, D. Kato, and S. Ohtani, *Phys. Rev. A* **63**, 032518 (2001).
- [51] S. A. Blundell, W. R. Johnson, M. S. Safronova, and U. I. Safronova, *Phys. Rev. A* **77**, 032507 (2008).
- [52] U. I. Safronova and M. S. Safronova, *J. Phys. B* **43**, 074025 (2010).
- [53] U. Safronova, A. S. Safronova, S. M. Hamasha, and P. Beiersdorfer, *At. Data Nucl. Data Tables* **92**, 47 (2006).
- [54] U. Safronova, A. S. Safronova, and P. Beiersdorfer, *J. Phys. B* **39**, 4491 (2006).
- [55] S. G. Porsev, Yu. G. Rakhlina, and M. G. Kozlov, *Phys. Rev. A* **60**, 2781 (1999).
- [56] M. S. Safronova, W. R. Johnson, and A. Derevianko, *Phys. Rev. A* **60**, 4476 (1999).
- [57] W. R. Johnson, D. Kolb, and K.-N. Huang, *At. Data Nucl. Data Tables* **28**, 333 (1983).
- [58] G. Tachiev and C. Froese Fischer, The MCHF/MCDHF Collection; <http://atoms.vuse.vanderbilt.edu>